Revised Version
Ref. No. (1993)026

SIMULATION OF SLOSHING DYNAMICS INDUCED FORCES AND TORQUES ACTUATED ON DEWAR CONTAINER DRIVEN BY GRAVITY GRADIENT AND JITTER ACCELERATIONS IN MICROGRAVITY

R. J. Hung and H. L. Pan

The University of Alabama in Huntsville

Huntsville, Alabama 35899 USA

I. Introduction

Some experimental spacecraft use superconducting sensors for gyro read-out and so must be maintained at a very low temperature. The boil-off from the cryogenic liquid used to cool the sensors can also be used, as the Gravity Probe-B (GP-B) spacecraft does, as propellant to maintain attitude control and drag-free operation of the spacecraft[1]. The cryogenic liquid for such spacecraft is, however, susceptible to both slosh-like motion and non-axisymmetric configurations under the influence of various kinds of gravity jitter and gravity gradient accelerations. Hence, it is important to quantify the magnitude of the liquid-induced perturbations on the spacecraft. Dynamic behavior of liquids in a moving container under reduced gravity environment have been widely discussed by Abramson[2]. Here we use the example of the GP-B to investigate such perturbations by numerical simulations. For this spacecraft disturbances can be imposed on the liquid by atmospheric drag, spacecraft attitude control maneuvers, and the Earth's gravity gradient. More generally, onboard machinery vibrations and crew motion can also create disturbances. Recent studies[3-7] suggest that high frequency disturbances are relatively unimportant in causing liquid motions in comparison to low frequency ones. The results presented here confirm this conclusion.

After an initial calibration period, the GP-B spacecraft rotates in orbit at 0.1 rpm about the tank symmetry axis. For this rotation rate, the equilibrium liquid free surface shape is a "doughnut" configuration for all residual gravity levels of $10^{-6}g_o$ or less, as shown by experiments[8] and by numerical simulations[4-7]; furthermore, the superfluid behavior of the 1.8 K liquid helium used in GP-B eliminates temperature gradients and therefore such effects as Marangoni convection do not have to be considered. Classical fluid dynamics theory is used

as the basis of the numerical simulations here, since Mason's experiments[9] show that the theory is applicable for cryogenic liquid helium in large containers[10]. To study liquid responses to various disturbances, we investigate and simulate three levels of gravity jitter (10^{-6}, 10^{-7}, and $10^{-8}g_o$) each at three predominant frequencies (0.1, 1.0, and 10 Hz), combined with a gravity gradient appropriate for the GP-B orbit[11-13]. In this study, dynamical evolution of sloshing dynamics excited fluid forces and torque fluctuations exerted on the dewar container driven by the combined gravity gradient and jitter accelerations are also investigated and simulated.

II. Mathematical Model of the Simulation of Sloshing Dynamics Modulated Bubble Oscillations

Consider a closed circular dewar of an inner radius a_1 and an outer radius a_2; top and bottom dome of radius b; with height L, which is partially filled with a cryogenic liquid helium and the rest of the ullage is filled with a helium vapor. Density and viscosity of liquid helium and helium vapor are ρ_L, μ_L, ρ_v, and μ_v, respectively. Let us use cylindrical coordinates (r, θ, z), with corresponding velocity components (u, v, w), corresponding components of gravity gradient acceleration ($a_{gg,r}$, $a_{gg,\theta}$, $a_{gg,z}$), and corresponding jitter acceleration ($a_{gj,r}$, $a_{gj,\theta}$, $a_{gj,z}$). The whole fluid system is spinning in the z-axis with an angular velocity of ω and an angular acceleration of α. The governing equations for non-inertia frame spacecraft bound coordinates are illustrated in our recent studies[14,15], and will not be repeated in this paper. In these formulations, $2\rho\omega u$ and $2\rho\omega v$ denote the Coriolis forces; $\rho r\omega^2$, the centrifugal force; and $\rho r\alpha$, the angular acceleration of spinning motion.

In the computation of fluid forces, moment, viscous stress and angular momentum acting on the container wall of the spacecraft, one has to consider

those forces and moment in the inertia frame rather than the non-inertia frame. For the case of spinning motion in the z-axis, one has to transform those vectors from the non-inertia frame to the inertia frame as follows:

$$\begin{bmatrix} F_x' \\ F_y' \\ F_z' \end{bmatrix} = \begin{bmatrix} \cos\omega t & -\sin\omega t & 0 \\ \sin\omega t & \cos\omega t & 0 \\ 0 & 0 & 1 \end{bmatrix} \begin{bmatrix} F_x \\ F_y \\ F_z \end{bmatrix} \tag{1}$$

where the prime symbol denotes vectors in the inertia frame while those parameters without the prime symbol indicate vectors in the non-inertia frame.

In order to solve sloshing dynamic problems of liquid propellent systems in orbital spacecraft under microgravity environment, one has to solve the governing non-inertia frame equations[14,15] accompanied by a set of initial and boundary conditions. A detailed illustration of these initial and boundary conditions concerning sloshing dynamics of fluid systems in microgravity were precisely given in our recent studies[15,16] and will not be repeated in this paper. In this study, to show a realistic example of the simulation, a full scale GP-B spacecraft propellant dewar tank with an outer radius of 78 cm and an inner radius of 13.8 cm, top and bottom radius of 110 cm and a height of 162 cm has been used in the numerical simulation. The dewar tank is 80% filled with cryogenic liquid helium and the rest of the ullage is filled with helium vapor. The temperature of cryogenic helium is 1.8 K. In this study the following data was used: liquid helium density = 0.146 g/cm^3, helium vapor density = 0.00147 g/cm^3, fluid pressure = 1.66 x 10^4 dyne/cm^2, surface tension coefficient at the interface between liquid helium and helium vapor = 0.353 dyne/cm, liquid helium viscosity coefficient = 9.61 x 10^{-5} cm^2/s; and contact angle = 0°. The initial interface profiles of the liquid-vapor-solid phase used in this study have been given explicitly through the steady state computations made by Hung and Leslie[17]

and Hung et al.[4,5,17], which were checked by the experiments carried out by Leslie[8].

A staggered grid for the velocity components is used in this computer program. The marker-and-cell method of studying fluid flows along a free surface is adopted[18-21]. The formulation for this method is valid for any arbitrary interface location between the grid points and is not limited to middle point interfaces[20].

There are several methods to be used to solve fluid flow simulation problems in a free surface. Explicit, semi-explicit and implicit schemes are the most commonly used methods. Mixing methods for these schemes are employed in this study. A near semi-implicit PCMI method (Predictor-Corrector Multiple-Interaction Technique)[22] is used to simulate velocity profiles, and Gauss-Seidel[22], or Conjugate Gradient[24] methods are employed to simulate pressure iteration, while Successive Over-Relaxation method[25] is used to simulate free surface configurations through iteration. It has been shown that near semi-implicit scheme for PCMI method is more reliable than that of the explicit scheme, and also more convenient and computational time saving than that of the implicit scheme[26]. Second order accuracy of derivatives are adopted in the finite-different equations while the truncation errors for the interior of time and spatial steps are of (Δt^2) and $(\Delta r^2, \Delta \theta^2, \Delta z^2)$, respectively. The convergence criteria for velocity, pressure and liquid volume are less than 10^{-5}. Some of the steady state computational results are compared with the experimental observations carried over by Leslie[8] in free-falling aircraft (KC-135) with excellent agreement.

III. Simulation of Bubble Oscillations Driven by Gravity Gradient and Jitter Accelerations

With an example of the GP-B Spacecraft, which is an Earth satellite orbiting at 650 km altitude directly over the poles, the orbit period, τ_o can be computed from following expression:

$$\tau_o = 2\pi \frac{R_c^{3/2}}{R_E g_o^{1/2}} \tag{2}$$

where R_E denotes radius of Earth (= 6373 km); R_c, radius of circular orbit (= R_E + h = 7023 km); h, orbit altitude (= 650 km); and g_o, Earth gravity acceleration (= 9.81 $^m/s^2$). For the case of GP-B, the orbit period τ_o = 97.6 min, and orbit rate n = $^{2\pi}/\tau_o$ = 1.07 x 10^{-3} $^{rad}/_s$.

The gravity gradient acceleration acting on the fluid mass of spacecraft can be shown as[12,27]

$$\hat{a}_{gg} = -n^2 [3 (\hat{r}_c \cdot \hat{d}) \hat{r}_c - \hat{d}] \tag{3}$$

where $\hat{a}_{gg}$ denotes gravity gradient acceleration vector; $\hat{d}$, vector from the fluid element to the spacecraft geometric center; $\hat{r}_c$, unit vector from the spacecraft geometric center to the center of the Earth; and n, the orbit rate.

For the case of the GP-B Spacecraft, it is assumed that the gravity exerted on the mass center of the spacecraft orbiting around the Earth on its specified orbit is zero. In other words, all the gravity acceleration exerted on the spacecraft is nothing but the gravity gradient acceleration which is defined in Equation (3).

Figure 1 illustrates the geometrical relationship of the parameters shown in Equation (3). Let us consider the fluid element of interests, m, located at (r, θ, z) in cylindrical coordinates and at (x, y, z) in cartesian coordinates. As $|\hat{d}|$ is much smaller than the distance between the location of the GP-B Spacecraft mass center to the center of the Earth, $\hat{r}_c$ through the GP-B geometric

center and $\hat{r}_c$ through the fluid element, m, is basically the same.

The gravity gradient acceleration acted on the fluid element located at (r, θ, z), in non-inertia frame coordinates is shown as follows[14,15]:

$$\hat{a}_{gg} = \begin{bmatrix} a_{gg,r} \\ a_{gg,\theta} \\ a_{gg,z} \end{bmatrix} = -n^2 \begin{bmatrix} \cos(\theta+\omega t) & \sin(\theta+\omega t) & 0 \\ -\sin(\theta+\omega t) & \cos(\theta+\omega t) & 0 \\ 0 & 0 & 1 \end{bmatrix} \cdot$$

$$\cdot \begin{bmatrix} 3[(z-L/2)\cos\psi_E - r\cos(\theta+\omega t)\cdot\sin\psi_E]\sin\psi_E + r\cos(\theta+\omega t) \\ r\sin(\theta+\omega t) \\ -3[(z-L/2)\cos\psi_E - r\cos(\theta+\omega t)\cdot\sin\psi_E]\cos\psi_E + (z-L/2) \end{bmatrix} \quad (4)$$

where ψ_E denotes the azimuth angle of Earth toward the location of spacecraft geometric center, or angle between spacecraft rotating axis and radial direction from spacecraft geometric center to center of Earth; n, the orbit rate; and t, the time of spacecraft orbiting around the Earth.

At time t = 0, the rotating axis of spacecraft is aligned with the radial direction of Earth center to the spacecraft mass center. Assuming spacecraft axis of rotating is linearly turning around 0° to 360° in 1200 s when spacecraft is orbiting around the Earth. Thus, ψ_E can be defined as

$$\psi_E = 2\frac{\pi}{\tau}t \quad (5)$$

where τ is spacecraft gravity turn-around time (= 1200 s in this case); and t is the time measured from the instant when the direction of spacecraft rotating axis is aligned with the radial direction of spacecraft mass center to the center of the Earth.

Fluctuations of residual gravity due to gravity jitter acceleration is modeled by following equation[11]:

$$g = g_B[1 + \frac{1}{2}\sin(2\pi f t)] \tag{6}$$

where g_B denotes the background gravity environment, and f(Hz) stands for the frequency of gravity-jitters.

In this study, three ranges of gravity jitter background with gravity of 10^{-6}, 10^{-7} and 10^{-8} g_o due to different intensity of spacecraft atmospheric drag and rotating speed of 0.1 rpm for normal GP-B spacecraft operation, and three frequencies of gravity jitter with the values of 0.1, 1.0 and 10 Hz have been considered for the investigation of the oscillations of the liquid-vapor interface. Components of gravity jitter acceleration in non-inertia coordinate system shall be given by[11,14,15]

$$\hat{a}_{gj} = (a_{gj,r}, a_{gj,\theta}, a_{gj,z}) = [g\sin\psi_E\cos(\theta+\omega t), -g\sin\psi_E\sin(\theta+\omega t), -g\cos\psi_E] \tag{7}$$

The characteristics of gravity gradient and jitter accelerations, shown in Equations (4) and (7), respectively, are quite different. Gravity gradient acceleration indicates that acceleration acted on any fluid mass inside the container increases two units of acceleration per unit of distance measured from the mass center of the container (point O_s at Figure 1) to the location of the fluid mass parallel along the radial axis from the mass center of the container to the center of the Earth (parallel to unit vector $\hat{r}_c$ shown in Figure 1) while the acceleration acted on the fluid mass decreases one unit of acceleration per unit of the shortest distance measured from the location of the fluid mass to the radial axis along the vector from the mass center of the container to the center of the Earth[12]. To give an example, Figure 2 shows the time variation of gravity gradient accelerations for a turn-around period of 1200s with container rotating speed of 0.1 rpm for components along (x, y, z) directions acted on the fluid

mass located at (r, θ, z) = (60 cm, $\pi/4$, 40 cm). As the magnitude and direction of gravity gradient acceleration acted on each fluid mass is strongly dependent upon how far the location of the fluid mass deviates from the mass center of the container measured along the axis parallel to the vector $\hat{r}_c$ which varies with respect to time, it can be anticipated that gravity gradient acceleration acted on the fluid mass is different for fluid mass at different locations in the container. Figure 2 shows that the magnitude of gravity gradient acceleration is on the order of 10^{-7} g_o. On the contrary to gravity gradient acceleration which acts different acceleration on the fluid mass at different locations in the container, gravity jitter acceleration drives the same acceleration on the fluid mass at different locations in the container. Figure 3 shows the time variation of gravity jitter accelerations for a turn-around period of 1200 s with a container rotating speed of 0.1 rpm and a jitter frequency of 0.1 Hz for components along (x, y, z) directions acted on the fluid mass everywhere in the container. It is shown in Figure 2 that gravity gradient accelerations are on the order of 10^{-7} g_o for the spacecraft orbit chosen in this example, three ranges of background gravity, 10^{-6}, 10^{-7} and 10^{-8} g_o for gravity jitter accelerations correspond to the magnitude of acceleration higher, equal, and lower, respectively, than that of the gravity gradient acceleration acted on the fluid system of the spacecraft.

The equilibrium shape of the liquid-vapor interface for a rotating dewar under a residual gravity environment below $10^{-6}g_o$ and rotating speed of 0.1 rpm is very much alike and is a doughnut configuration with a near circular kidney-shape cross-section based on the computation of the numerical algorithm developed in our earlier studies[4]. Figure 4(A) shows the initial shape of the interface in the r-z plane at θ = 0° and 180°; Figure 4(B) shows the initial profile of the

liquid-vapor interface in the r-z plane at θ = 90° and 270°; Figure 4(C) shows the initial profile of the liquid-vapor interface in the r-θ plane at height z = 108 cm; and Figure 4(D) shows the initial profile of three-dimensional liquid-vapor interface. Becuase of page limitation, the time evolution of three-dimensional bubble oscillations only will be illustrated in this paper.

In this study, combined gravity gradient and three ranges of jitter (10^{-6}, 10^{-7}, and 10^{-8} g_o) accelerations acting on the liquid-vapor interface oscillations have been simulated and investigated.

(III-A) Combined Gravity Gradient and 10^{-8} g_o Jitter Accelerations Acting on Bubble Oscillations

In this case, combined effects of gravity gradient and jitter accelerations are completely dominated by the gravity gradient acceleration when the 10^{-8} g_o and less gravity jitter accelerations are applied simultaneously with gravity gradient acceleration (which is on the order of 10^{-7} g_o as shown in Figure 2) for the excitation of slosh waves along liquid-vapor interface oscillations.

Figure 5 shows the time sequence evolution of the bubble profiles driven by these combined accelerations. For the convenience of comparison, figures of liquid-vapor interface profiles with the same values of the time sequences chosen throughout this paper are at time t = 191, 354, 380, 431, 503, 603, 825, 980, 995, 1050, 1080 and 1200 s. It clearly shows that there are a series of asymmetric oscillations excited along the surface of liquid-vapor interface driven by asymmetric gravity gradient-dominated acceleration.

Careful examination for the case of gravity gradient-dominated acceleration-effected liquid-vapor interface oscillations, gravity gradient acceleration shown in Equation (3), indicate that there are greater negative components of acceleration longitudinal to the direction aligned with spacecraft

mass center to the Earth center, and smaller positive components of acceleration transverse to this direction. As we indicated in Equation (5), angle ψ_E varies with time. This phenomena shows that gravity gradient acceleration exerted on the spacecraft is equivalent to the combination of time dependent force with turn-around direction and torsional moment acting on the spacecraft when it is orbiting around the Earth. It shows in Figures 4 and 5 that the deformation of the bubble is created by an asymmetric torsional moment with a twisting force.

Figure 5 shows the time sequence evolution of the three-dimensional dynamical behavior of the bubble oscillations driven by gravity gradient-dominated acceleration. Left-side up and right-side down oscillations of bubble in the vertical cross-section of doughnut profiles indicate a very important characteristics of gravity gradient-dominated acceleration which produce a combination of time dependent equivalent-torsional moment and twisting force acting on the spacecraft when it is orbiting around the Earth.

(III-B) Combined Gravity Gradient and 10^{-7} g_o Jitter Accelerations Acting on Bubble Oscillations

In this section, combined effects of accelerations are equally weighted by both the gravity gradient and jitter accelerations when 10^{-7} g_o gravity jitter acceleration is jointly applied simultaneously with gravity gradient acceleration (which is on the order of 10^{-7} g_o as shown in Figure 2) for the excitation of slosh waves along the liquid-vapor interface oscillations. Figure 6 shows the time sequence evolution of dynamical behavior of the bubble oscillations driven by these combined accelerations. Similar to Figure 5, same values of the time sequences are chosen. It also shows that there are a series of asymmetric oscillations excited along the surface of liquid-vapor interface driven by asymmetric equally weighted gravity gradient and jitter accelerations.

As we recorded in Figure 5, the effect of gravity gradient-dominated acceleration exerted on the spacecraft is equivalent to the combination of time-dependent force with turn-around direction of torsional moment acting on the spacecraft when it is orbiting around the Earth. On the other hand, it will be show later in Section (III-C) for the case of gravity jitter-dominated acceleration exerted on the spacecraft which is equivalent to time-dependent oscillatory forces that push the bubble in the combined directions of down-and-up and leftward-and-rightward as the bubble is rotating with respect to the spacecraft rotation axis. Figure 6 exactly illustrate these combined effects of equally weighted gravity gradient and jitter accelerations which drive the bubble in a manner of combined oscillations of the left-side-up, right-side-down and whole bubble down-and-up motions.

Figure 6 shows the time sequence evolution of the three-dimensional behavior of the liquid-vapor interface oscillations driven by equally weighted gravity gradient and jitter accelerations. A combined oscillations of left-side up and right-side down together with down-and-up bubble oscillations modified by leftward-and-rightward oscillations of bubble in the vertical cross-section of doughnut profiles indicates very important characteristics of combined gravity gradient and jitter accelerations of equal weight acting on the spacecraft when it is orbiting around the Earth.

(III-C) Combined Gravity Gradient and 10^{-6} g_o Jitter Accelerations Acting on Bubble Oscillations

In this case, combined effects of gravity gradient and jitter accelerations are completely dominated by the gravity jitter acceleration when the 10^{-6} g_o and higher gravity jitter acceleration are applied simultaneously with gravity gradient acceleration (which is on the order of 10^{-7} g_o as shown in Figure 2) for

the excitation of slosh wave along the liquid-vapor interface oscillations.

Figure 7 shows the time sequence evolution of the dynamical behavior of the bubble oscillations driven by gravity jitter-dominated acceleration of 0.1 Hz low jitter frequency. It clearly shows that there are a series of asymmetric oscillations excited along the surface of liquid-vapor interface driven by asymmetric gravity jitter-dominated acceleration.

Figure 7 shows the time sequence evolution of the three-dimensional dynamical behavior of the capillary effect governed interface oscillations driven by gravity jitter-dominated acceleration of 0.1 Hz low jitter frequency. It clearly shows that there are a series of asymmetric oscillations excited along the surface of liquid-vapor interface driven by asymmetric gravity jitter-dominated acceleration.

Careful examination for the case of gravity jitter acceleration-dominate liquid-vapor interface oscillations, gravity jitter acceleration, shown in Equations (6) and (7) which is also illustrated in Figure 3, indicate that there is a sinusoidal oscillation longitudinal to the direction aligned with spacecraft mass center to Earth center (parallel to unit vector $\hat{r}_c$ shown in Figure 1). As we indicated in Equation (5), the angle ψ_E varies with time. This phenomena shows that gravity jitter acceleration exerted on the spacecraft is equivalent to time-dependent oscillatory forces which push the bubble in the combined directions of down-and-up (see z-component of gravity jitter acceleration shown in Figure 3) and leftward-and-rightward (see x-and-y components of gravity jitter accelerations shown in Figure 3) as the bubble is rotating with respect to spacecraft rotation axis. Down-and-up motion of the bubble is due to the fact that z-component gravity jitter acceleration decreases from maximum downward direction to minimum downward direction, during the time period between $t = 0$ to

t = 300 s, which push liquid downward and bubble upward; while gravity jitter acceleration changes to its downward direction and magnitude from minimum upward to maximum upward, and then back to minimum upward, during the time periods between t = 300 s to t = 900 s, which push liquid upward and bubble downward; in the meanwhile, gravity jitter acceleration changes to its downward direction and magnitude during the period from t = 900 s to 1200 s which repeats the half cycle story of time period from t = 0 to t = 300 s. Leftward-and-rightward oscillations of bubble are the results of positive and negative directions of gravity jitter accelerations in x- and y-components as that illustrated in Figure 3. Positive direction gravity jitter acceleration implies that liquid is pushed rightward and the bubble is driven leftward. Time variations of gravity jitter accelerations, shown in Figure 3, characterize the leftward and rightward oscillations of bubbles shown in Figure 7.

In addition to the 0.1 Hz low frequency gravity jitter-dominated acceleration, 1.0 Hz medium frequency and 10 Hz high frequency gravity jitter acceleration driven liquid-vapor interface oscillations also have been investigated. Characteristics of these three ranges of gravity jitter frequencies have been well-documented in the earlier studies[3-6]. Because of page limitation, oscillations driven by the time-dependent variations of the direction of gravity jitter-dominated acceleration with medium and high frequencies will not be shown in this paper. Results show that lower frequency gravity jitter-dominated acceleration contribute more in the driving of asymmetric profiles of the interface than that of the higher frequency gravity jitter-dominated acceleration. These results are agreeable with the earlier studies[4-7].

VI. Mathematical Formulation of the Simulation of Sloshing Dynamics Induced Fluid Force and Torque Fluctuations

To model the simulation of forces and torques exerted on the dewar by large amplitude liquid motions, the fluid stresses are decomposed into tangential Π_t and normal Π_n components relative to the walls. These expressions are:

$$\Pi_t = \mu\left(\frac{\partial u_\alpha}{\partial x_\beta} + \frac{\partial u_\beta}{\partial x_\alpha}\right)\hat{t}_\alpha \hat{n}_\beta \tag{8}$$

$$\Pi_n = P\delta_{\alpha\beta} - \mu\left(\frac{\partial u_\alpha}{\partial x_\beta} + \frac{\partial u_\beta}{\partial x_\alpha}\right)\hat{n}_\alpha \hat{n}_\beta \tag{9}$$

where P is the thermodynamic pressure, u_α is the fluid velocity in the α direction, $\hat{n}_\alpha$ and $\hat{t}_\alpha$ are unit vectors normal and tangential to the walls, and $\delta_{\alpha\beta}$ is the Kronecker delta; subscripts α and β imply the directions. In the computation of how fluid force and torque fed back to the container, mathematical formulation of non-inertia frame (container bound coordinate) derived earlier have to be transformed back to inertia frame (Earth bound coordinate) to carry out the calculation[15,28]. Also, to accommodate the pitching, yawing, and rolling of the spacecraft, it is convenient here to use Cartesian coordinate (x, y, z) with corresponding velocity components. For GP-B, the axis of rotation is always fixed at the proof mass located at the mass center of the dewar (x_c, y_c, z_c) = (0, 0, L/2). Detailed derivations and expressions for the fluid-stress forces (F_x, F_y, F_z) and moments (M_x, M_y, M_z) are given in our recent work[15,28] and so will not be repeated here. The moment arm relating the forces and moments is given by:

$$\begin{bmatrix} L_x \\ L_y \\ L_z - L/2 \end{bmatrix} = \frac{1}{F_x^2 + F_y^2 + F_z^2}\begin{bmatrix} F_y M_z - F_z M_y \\ F_z M_x - F_x M_z \\ F_x M_y - F_y M_x \end{bmatrix} \tag{10}$$

where L_x, L_y, and L_z denote the components of the moment arm along x, y, and z axes, respectively.

V. Characteristics of the Simulation of Slosh Waves Induced Fluid Force and Torque Fluctuations Exerted on the Dewar Container

With references to Sections III and IV, one can calculate the fluid force and the associated torques exerted on the dewar container of spacecraft propellant tank.

(V-A) Combined Gravity Gradient and 10^{-8} Jitter Acceleration Driven Fluid Forces Fluctuations

As we mentioned earlier, the combined effects of gravity gradient and jitter accelerations are completely dominated by gravity gradient acceleration when the 10^{-8} g_o and less gravity jitter accelerations are applied simultaneously with gravity gradient acceleration which drive viscous stress and its moment fluctuations.

Figure 8 shows the computed time variation of the fluctuations of fluid forces exerted on the dewar container driven by gravity gradient-dominated acceleration. This figure shows the following results: (a) The values of fluid force fluctuations are $(\Delta F_x, \Delta F_y, \Delta F_z) = (23.7, 18.3, 61.7)$ dynes, it clearly indicates $\Delta F_z > \Delta F_x > \Delta F_y$. The maximum absolute values of fluid force are Max $(|F_x|, |F_y|, |F_z|) = (17.4, 11.5, 32.4)$ dynes. It also indicates $|F_z| > |F_x| > |F_y|$. (b) The initial values of F_x and F_y start from zero value while that of the F_z starts from non-zero value. This is due to the fact that the shape of rotating bubble is symmetric with respect to the x and y axes which makes F_x and F_y equal to zero at time $t = 0$ while the resultant force along the rotating axis of z is not equal to zero because of pre-existing gravity force acting along the z-axis at the very beginning. (c) The characteristics of fluid forces and their fluctuations are very much following the trend of dominated gravity gradient acceleration, shown in Figure 2. In other words, gravity gradient acceleration

as a major input force, modulated by sloshing dynamics of the fluid system in the dewar, activate on the dewar container with response force. In reality, the fluid system, modulated by sloshing dynamics, acts as a damper in the spacecraft to damp out the acting force of gravity gradient acceleration.

Figures 9(A), (B) and (C) show variations of fluid torque exerted on the dewar container due to slosh waves driven by gravity gradient-dominated acceleration along the x, y and z axes, respectively. The values of fluid torque fluctuations are $(\Delta M_x, \Delta M_y, \Delta M_z) = (761.9, 667.3, 0.06)$ dyne·cm. The maximum absolute values of fluid torque are Max $(|M_x|, |M_y|, |M_z|) = (392.9, 343.4, 0.50)$ dyne·cm. It shows $\Delta M_x > \Delta M_y > \Delta M_z$ and $|M_x| > |M_y| > |M_z|$. As M_y, M_x, M_z are determined by the Factors (F_x, L_z, F_z, L_x), (F_z, L_y, F_y, L_z) and (F_y, L_x, F_x, L_y), respectively, it was illustrated in Figures 8 and 10 that the magnitudes of force fluctuations give $|F_z| > |F_x| > |F_y|$ and that of moment arm fluctuations give $|L_z| > |L_x| > |L_y|$ in which time averages of L_x and L_y were approaching zero. This explains why the moment of $M_z = L_xF_y - L_yF_x \sim 0$ even though there is a rolling moment with angular velocity of 0.1 rpm in which the induced rolling moment exerted by the viscous rotating fluids is small in comparison with the induced pitch and yaw moments due to asymmetric slosh wave excitation.

Figure 10 shows time fluctuations of moment arms of fluid torques exerted on the dewar container due to slosh waves excited by gravity gradient-dominated acceleration. The values of moment arm fluctuations are $(\Delta L_x, \Delta L_y, \Delta L_z) = (22.8, 19.0, 45.5)$ cm. The maximum absolute values of moment arm are Max $(|L_x|, |L_y|, |L_z|) = (12.2, 10.2, 103.4)$ cm. It shows $\Delta L_z > \Delta L_x > \Delta L_y$ and $|L_z| > |L_x| > |L_y|$. This trend is very much similar to the driving force of gravity gradient acceleration, shown in Figure 2.

(V-B) Combined Gravity Gradient and 10^{-7} Jitter

Acceleration Driven Fluid Forces Fluctuations

As we mentioned earlier, the combined effects of accelerations are equally weighted by both the gravity gradient and jitter accelerations when 10^{-7} g_o gravity jitter acceleration is jointly applied simultaneously with gravity gradient acceleration which drive viscous stress and its moment fluctuations.

Fluctuations of fluid force, fluid torque and moment arm of fluid torques driven by gravity jitter acceleration with frequencies of 0.1 , 1.0 and 10 Hz have been simulated and investigated. Because of page limitation, results of fluctuations driven by 0.1 Hz gravity jitter frequency only will be presented in this study. Figure 11 shows the computed time variation of the fluctuations of fluid force exerted on the dewar container driven by equally weighted gravity gradient and jitter accelerations with a frequency of 0.1 Hz. The values of fluid force fluctuations are (ΔF_x, ΔF_y, ΔF_z) = (62.4, 57.6, 110.4) dynes and the maximum absolute values of fluid force are Max ($|F_x|$, $|F_y|$, $|F_z|$) = (33.0, 32.3, 68.1) dynes. It shows $\Delta F_z > \Delta F_x > \Delta F_y$ and $|F_z| > |F_x| > |F_y|$. Comparison between Figures 8 and 11 for fluid force fluctuations driven by gravity gradient-dominated acceleration and equal weight gravity gradient and jitter accelerations show that they are in the same order, and it also shows that equal weight gravity gradient and jitter accelerations excited values and fluctuations of fluid force exerted on the dewar container have a greater value of magnitudes than that driven by gravity gradient-dominated acceleration. Comparison among Figures 2,3 and 11 show that Figure 11 is equally modulated by Figures 2 and 3. In other words, the response of sloshing dynamics modulated forces are equally influenced by both gravity gradient and jitter accelerations with smaller amplitudes of fluctuations due to sloshing dynamics.

Figures 12(A), (B) and (C) show variations of fluid torques exerted on the

container wall due to slosh waves excited by equal weight gravity gradient and jitter acceleration with frequency of 0.1 Hz along the x, y and z axes, respectively. The values of fluid torque fluctuations are (ΔM_x, ΔM_y, ΔM_z) = (1038.8, 823.2, 0.07) dyne·cm and the maximum absolute values of fluid torque are Max ($|M_x|$, $|M_y|$, $|M_z|$) = (538.5, 484.7, 0.50) dyne·cm. It shows $\Delta M_x > \Delta M_y > \Delta M_z$ and $|M_x| > |M_y| > |M_z|$. Characteristics of the fluctuations of fluid torques driven by equal weight gravity gradient and jitter accelerations are similar to that drawn for the fluctuations of fluid torques driven by gravity gradient-dominated acceleration with greater amplitudes and fluctuations.

Figure 13 shows time fluctuations of moment arm of fluid torque exerted on the dewar container due to slosh waves excited by equal weight gravity gradient and jitter accelerations. The values of moment arm fluctuations are (ΔL_x, ΔL_y, ΔL_z) = (20.3, 14.8, 33.3) cm. The maximum absolute values of moment arm are Max ($|L_x|$, $|L_y|$, $|L_z|$) = (11.5, 9.3, 99.0) cm. It shows $\Delta L_z > \Delta L_x > \Delta L_y$ and $|L_z| > |L_x| > |L_y|$.

(V-C) Combined Gravity Gradient and $10^{-6}g_o$ Jitter Accelerations Driven Fluid Forces Fluctuations

As we mentioned earlier, the combined effects of gravity gradient and jitter accelerations are completely dominated by the gravity jitter acceleration[16] when the 10^{-6} g_o and higher jitter acceleration are applied simultaneously with gravity gradient acceleration which drive fluid force and its torque fluctuations.

Figure 14 shows the computed time variation of the fluctuations of fluid force exerted on the dewar container driven by gravity jitter-dominated acceleration with a frequency of 0.1 Hz. The values of fluid force fluctuations are (ΔF_x, ΔF_y, ΔF_z) = (383.0, 315.5, 619.7) dynes and the maximum absolute values

of fluid force are Max ($|F_x|$, $|F_y|$, $|F_z|$) = (192.2, 172.3, 359.5) dynes. It shows $\Delta F_z > \Delta F_x > \Delta F_y$ and $|F_z| > |F_x| > |F_y|$. Comparison of input and response of forces between Figures 3 and 14 show that these two sets of curves are very much similar in characteristics and trends with smaller amplitudes and fluctuations shown in the response curve. In other words, it indicates that the fluid system, with modulation of sloshing dynamics, acts as a damping machine in input and response circuit. Comparison between Figures 8 and 14 for fluid force fluctuations driven by gravity gradient-dominated acceleration and gravity jitter-dominated acceleration show that gravity jitter-dominated acceleration are responsible for the excitation of greater values and magnitudes than that driven by gravity gradient-dominated acceleration.

Figures 15(A), (B) and (C) show variations of fluid torque exerted on the container wall due to slosh waves excited by gravity jitter-dominated acceleration with frequency of 0.1 Hz along the x, y and z axes, respectively. The values of fluid torque fluctuations are (ΔM_x, ΔM_y, ΔM_z) = (1612.2, 1957.9, 0.10) dyne·cm and the maximum absolute values of fluid torque are Max ($|M_x|$, $|M_y|$, $|M_z|$) = (1013.7, 1139.3, 0.52) dyne·cm. It shows $\Delta M_y > \Delta M_x > \Delta M_z$ and $|M_y| > |M_x| > |M_z|$. Characteristics of the fluctuations of fluid torques driven by gravity jitter-dominated acceleration are similar to that drawn for the fluctuations of fluid torque driven by gravity jitter-dominated acceleration. However, gravity jitter-dominated acceleration excited values and fluctuations of fluid torque exerted on the dewar container have a greater value and magnitude than that driven by gravity gradient-dominated acceleration.

Figure 16 shows time fluctuations of moment arm of fluid torque exerted on the dewar container due to slosh waves excited by asymmetric gravity jitter-dominated acceleration. The values of moment arm fluctuations are (ΔL_x, ΔL_y,

ΔL_z) = (4.6, 3.9, 5.3) cm. The maximum absolute values of moment arm are Max ($|L_x|$, $|L_y|$, $|L_z|$) = (2.4, 3.3, 77.8) cm. It shows $\Delta L_z > \Delta L_y > \Delta L_x$, and $|L_z| > |L_y| > |L_x|$. Comparison of gravity gradient-dominated and gravity jitter-dominated accelerations driven fluctuations provide the following conclusions: (a) Torsional moment-and twisting force-equivalent gravity gradient-dominated acceleration exerted on the rotating dewar container produces smaller order of values and fluctuations of fluid force and fluid torque than that driven by gravity jitter-dominated acceleration. (b) Dynamics of bubble (liquid-vapor interface) driven by torsional moment-and twisting force-equivalent gravity gradient-dominated acceleration produces greater fluctuations and magnitude of fluid moment arm than that produced by up and down oscillations of bubble driven by gravity jitter-dominated acceleration. (c) Input and response relation between combined gravity gradient/jitter accelerations and fluid forces activated on the dewar container through the modulation of sloshing dynamics show that the characteristics and trends are similar. However, the fluid system acts a damper which, in a realistical sense, helps damping out the spacecraft acceleration activated by the orbital forces.

V. Discussion and Conclusion

Dynamics of spacecraft disturbances activated by the imbalance of liquid propellant[29,30] driven by gravity gradient-dominated and gravity jitter-dominated accelerations, in particular the actuation of the disturbances of spacecraft dynamics through the effect of surface tension on partially-filled rotating dewar containers (liquid helium and helium vapor) with time-dependent microgravity environment have been carried out by numerically computing the three-dimensional non-inertia frame Navier-Stokes equations subject to the initial and boundary conditions. The initial condition for the liquid-vapor interface profiles were

adopted from the steady-state formulation of rotating dewar developed by Hung and Leslie[17].

In this study, spacecraft gravity turn-around time is assumed to be 1200s. The equivalent twisting force and torsional moment of gravity gradient-dominated acceleration, acted on the rotating dewar orbiting around the Earth, induce left-side-up and right-side-down in the horizontal cross section of doughnut profiles. For the case of bubble oscillations driven by gravity jitter-dominated acceleration, up-and-down and leftward-and-rightward motion have been resulted.

Fluid force and fluid torque moment exerted on the dewar wall along the yawing and pitching axes caused by slosh wave excitation driven by gravity gradient-dominated and gravity jitter-dominated accelerations in partially liquid-filled container, in addition to the existing rotating motion along the rolling axes, have been simulated and investigated. Results show that there are a series of large amplitude fluctuation of fluid forces, fluid torque and moment arms exerted on the dewar container of spacecraft propellant tank which in turn disturb the dynamics of spacecraft along yawing and pitching axes. In particular, slosh waves excited by the asymmetry gravity gradient-dominated and gravity jitter-dominated accelerations contribute greatly to the large amplitude fluctuations of fluid forces and fluid torque exerted on the container and the dynamics of spacecraft along the pitching and yawing axes, in addition to the existing rolling axis of spacecraft[29,30].

Time-dependent variations in the direction of gravity gradient-dominated and gravity jitter-dominated accelerations imposed on the spacecraft will change and modify the asymmetry distribution of liquid-vapor in the rotating dewar container and the dynamic system of spacecraft[31]. This means that the dynamic system of spacecraft through the fluid forces and fluid torque exerted on the

container wall will be deeply disturbed by the presence of asymmetric fluctuations in liquid-vapor interface[29,30]. In this study, the differences in gravity gradient-dominated acceleration and gravity jitter-dominated acceleration induced slosh waves and how these slosh wave excitation affected the dynamic system of spacecraft through the fluctuations in fluid force and fluid torque exerted on the container wall distribution have been simulated and studied.

Acknowledgement

The authors appreciate the support received from the National Aeronautics and Space Administration through the NASA Grant NAG8-938 and NASA Contract NAS8-38609/Delivery Order No. 103. They would like to express their gratitude to Richard A. Potter of NASA/Marshall Space Flight Center for the stimulating discussions during the course for the present study.

References

1. Wilkinson, D. T., Bender, P. L., Eardley, D. M., Gaisser, T. K., Hartle, J. B., Israel, M. H., Jones, L. W., Partridge, R. B., Schramm, D. N., Shapiro, I. I., Vessort, R. F. C., and Wagoner, R. V., Gravitation, Cosmology and Cosmic-Ray Physics, Physics Today, 39, 43-46, 1986.

2. Abramson, N. H., The Dynamical Behavior of Liquids in a Moving Container, NASA SP-106, NASA, Washington, D. C., 1966.

3. Kamotani, Y., Prasad, A., and Ostrach, S., Thermal Convection in an Enclosure Due to Vibrations Aboard a Spacecraft, AIAA Journal, 19, 511-516, 1981.

4. Hung, R. J., Lee, C. C., and Leslie, F. W., Response of Gravity Level Fluctuations on the Gravity Probe-B Spacecraft Propellant System, Journal of Propulsion and Power, 7, 556-564, 1991.

5. Hung, R. J., Lee, C. C., and Leslie, F. W., Effect of the Baffle on the Spacecraft Fluid Propellant Viscous Stress and Moment Fluctuations, Transaction of the Japan Society for Aeronautical and Space Sciences, 35, 187-207, 1993.

6. Hung, R. J., and Shyu, K. L., Space-Based Cryogenic Liquid Hydrogen Reorientation Activated by Low Frequency Impulsive Reverse Thruster of Geyser Initiation, Acta Astronautica, 25, 709-719, 1991.

7. Hung, R. J., and Shyu, K. L., Constant Reverse Thrust Activated Reorientation of Liquid Hydrogen with Geyser Initiation, Journal of Spacecraft and Rockets, 29, 279-285, 1992.

8. Leslie, F. W., Measurements of Rotating Bubble Shapes in a Low Gravity Environment, Journal of Fluid Mechanics, 161, 269-279, 1985.

9. Mason, P., Collins, D., Petrac, D., Yang, L., Edeskuty, F., Schuch, A., and

Williamson, K., The Behavior of Superfluid Helium in Zero Gravity, Proc. 7th International Cryogenic Engineering Conferences, Surrey, England, Science and Technology Press, 1978.

10. Hung, R. J., Pan, H. L., and Long, Y. L., Peculiar Behavior of Helium II Disturbances Due to Sloshing Dynamics Driven by Jitter Acceleration Associated with Slew Motion in Microgravity, Cryogenics, in press, 1994.

11. Avduyevsky, V. S. (editor), Scientific Foundations of Space Manufacturing, MIR, Moscow, USSR, 1984.

12. Forward, R. L., Flattening Space-Time Near the Earth, Physical Review, Series (A), 26, 735-744, 1982.

13. Misner, C. W., Thorne, K. S., and Wheeler, J. A., Gravitation, W. H. Freeman and Co., San Francisco, CA, pp. 1-1279, 1973.

14. Hung, R. J., and Pan, H. L., Differences in Gravity Gradient and Gravity Jitter-Excited Slosh Waves in Microgravity, Transactions of the Japan Society for Aeronautical and Space Sciences, 36, 153-169, 1993.

15. Hung, R. J., Pan, H. L., and Leslie, F. W., Gravity Gradient or Gravity Jitter Induced Viscous Stress and Moment Fluctuations in Microgravity, Fluid Dynamics Research, in press, 1994.

16. Hung, R. J., and Pan, H. L., Asymmetric Slosh Wave Excitation in Liquid-Vapor Interface Under Microgravity, Acta Mechanica Sinica, 9(4), 298-311, 1993.

17. Hung, R. J., and Leslie, F. W., Bubble Shapes in a Liquid-Filled Rotating Container Under Low Gravity, Journal of Spacecraft and Rockets, 25, 70-74, 1988.

18. Harlow, F. H., and Welch, F. E., Numerical Calculation of Time-Dependent Viscous Incompressible Flow of Fluid with Free Surface, Physics of Fluids,

8, 2182-2189, 1965.

19. Patanker, S. V., Numerical Heat Transfer and Fluid Flow, Hemisphere-McGraw-Hill, New York, NY, pp. 197, 1980.

20. Patanker, S. V., and Spalding, S. D., A Calculation Procedure for Heat, Mass and Momentum Transfer in Three Dimensional Parabolic Flows, International Journal of Heat Mass Transfer, 15, 1787-1805, 1972.

21. Spalding, D. B. A Novel Finite-Difference Formulation for Differential Expressions Involving Both First and Second Derivatives, International Journal of Numerical Methods in Engineering, 4, 551-559, 1972.

22. Rubin, S. G., and Lin, T. C., A Numerical Method for Three-Dimensional Viscous Flow: Application to the Hypersonic Leading Edge, Journal of Computational Physics, 9, 339-364, 1972.

23. Salvadori, M. G., and Baron, M. L., Numerical Methods in Engineering, Prentice-Hall, Inc., Engloewood Cliffs, NJ, 1961.

24. Hageman, L. A., and Young, D. M., Applied Iterative Methods, Academic Press, New York, 1981.

25. Young, D., Iterative Methods for Solving Partial Differential Equations of Elliptical Type, Transactions of American Mathematical Society, 76, 92-111, 1954.

26. Kitchens, C. W., Jr., Navier-Stokes Solutions for Spin-Up in a Filled Cylinder, AIAA Journal, 188, 929-934, 1980.

27. Hughes, P. C., Spacecraft Attitude Dynamics, John Wiley and Sons, New York, 564, 1986.

28. Hung, R. J., Lee, C. C., and Leslie, F. W., Effect of the Baffle on the Spacecraft Fluid Propellant Viscous Stress and Moment Fluctuations, Transactions of the Japan Society for Aeronautical and Space Sciences,

35, 187-207, 1993.

29. Hung, R. J., Lee, C. C., and Leslie, F. W., Spacecraft Dynamical Distribution of Fluid Stresses Activated by Gravity Jitters Induced Slosh Waves, Journal of Guidance, Control and Dynamics, 15, 817-824, 1992.

30. Hung, R. J., and Pan, H. L., Fluid Force Activated Spacecraft Dynamics Driven by Gravity Gradient and Jitter Accelerations, Journal of Guidance, Control and Dynamics, 17, in press, 1994.

31. Hung, R. J., and Lee, C. C., Effect of Baffle on Gravity Gradient Acceleration Excited Slosh Waves in Microgravity, Journal of Spacecraft and Rockets, 31, in press, 1994.

Figure Captions

Figure 1 Coordinate system for the computation of gravity gradient acceleration, 0_g is the location of geometric center of cylinder. Direction of $\hat{r}_c$ points toward Earth center. (x', y', z') denotes absolute coordinate system, while (x, y, z) illustrates non-inertia frame spacecraft bound coordinate system.

Figure 2 Time variation of gravity gradient acceleration acting on fluid mass located at $(r, \theta, z) = (40\ cm, \pi/4, 10\ cm)$ for turn-around period of 1200 s with rotating speed of 0.1 rpm. (A) Along x-direction; (B) Along y-direction; (C) Along z-direction.

Figure 3 Time variation of gravity jitter acceleration acting on the fluid system with a value of 10^{-8}, 10^{-7} and 10^{-6} g_o, rotating speed of 0.1 rpm, turn-around period of 1200 s and gravity jitter frequency of 0.1 Hz. (A) Along x-direction; (B) Along y-direction; (C) Along z-direction.

Figure 4 Initial profiles of liquid-vapor interface for Gravity Probe-B module of rotating dewar with gravity of 10^{-7} g_o, rotating speed of 0.1 rpm and direction of background gravity at $\psi_E = 0°$. (A) In r-z plane at $\theta = 0°$ and 180°, (B) In r-θ plane at $\theta = 90°$ and 270°, (C) In r-θ plane at $z = 108$ cm, and (D) Three-dimensional liquid-vapor interface profile.

Figure 5 Time sequence evolution of three-dimensional liquid-vapor interface oscillations for rotating dewar driven by combined gravity gradient and jitter accelerations with gravity of 10^{-8} g_o. Rotating speed of dewar is 0.1 rpm, and the period of gravity direction turn-around time is 1200 s.

Figure 6 Time sequence evolution of three-dimensional liquid-vapor interface oscillations for rotating dewar driven by combined gravity gradient and jitter accelerations of 0.1 Hz frequency, gravity of 10^{-7} g_o with the period of gravity direction turn-around time = 1200 s, and rotating speed of 0.1 rpm.

Figure 7 Time sequence evolution of three-dimensional liquid-vapor interface oscillations for rotating dewar driven by combined gravity gradient and jitter accelerations of 0.1 Hz frequency, gravity of 10^{-6} g_o with the period of gravity direction turn-around time = 1200 s, and rotating speed of 0.1 rpm.

Figure 8 Time sequence of the fluctuations of fluid stress forces exerted on the dewar container due to the slosh wave excitation driven by combined gravity gradient and jitter accelerations with 10^{-8} g_o under rotating speed of 0.1 rpm and gravity turn-around time of 1200 s. (A) Along x-direction; (B) Along y-direction; and (C) Along z-direction.

Figure 9 Time sequence of the fluctuations of fluid stress moment exerted on the dewar container due to the slosh wave excitation driven by combined gravity gradient and jitter accelerations with 10^{-8} g_o under rotating speed of 0.1 rpm and gravity turn-around time of 1200 s. (A) Along x-direction; (B) Along y-direction; and (C) Along z-direction.

Figure 10 Time sequence of the fluctuations of moment arm of viscous stress moment exerted on the dewar container due to the slosh wave excitation driven by combined gravity gradient and jitter accelerations with 10^{-8} g_o under rotating speed of 0.1 rpm and

gravity turn-around time of 1200 s. (A) Along x-direction (pitching moment); (B) Along y-direction (yawing moment);and (C) Along z-direction (rolling moment).

Figure 11 Time sequence of the fluctuations of fluid stress moments exerted on the dewar container due to the slosh wave excitation driven by combined gravity gradient and jitter accelerations with 10^{-7} g_o, rotating speed of 0.1 rpm, gravity turn-around time of 1200 s and gravity jitter frequency of 0.1 Hz. (A) Along x-direction (pitching moment); (B) Along y-direction (yawing moment); and (C) Along z-direction (rolling moment).

Figure 12 Time sequence of the fluctuations of fluid stress moments exerted on the dewar container due to the slosh wave excitation driven by combined gravity gradient and jitter accelerations with 10^{-7} g_o rotating speed of 0.1 rpm, gravity turn-around time of 1200 s and gravity jitter frequency of 0.1 Hz. (A) Along x-direction fluid stress moment; (B) Along y-direction fluid stress moment; and (C) Along z-direction fluid stress moment.

Figure 13 Time sequence of the fluctuations of moment arm of fluid stress moments exerted on the dewar container driven by combined gravity gradient and jitter accelerations with 10^{-7} g_o, rotating speed of 0.1 rpm, gravity turn-around time of 1200 s and gravity jitter frequency of 0.1 Hz. (A) x-direction moment arm; (B) y-direction moment arm; and (C) z-direction moment arm.

Figure 14 Time sequence of the fluctuations of fluid stress moments exerted on the dewar container due to the slosh wave excitation driven by combined gravity gradient and jitter accelerations with 10^{-7} g_o,

rotating speed of 0.1 rpm, gravity turn-around time of 1200 s and gravity jitter frequency of 0.1 Hz. (A) Along x-direction (pitching moment); (B) Along y-direction (yawing moment); and (C) Along z-direction (rolling moment).

Figure 15 Time sequence of the fluctuations of fluid stress moments exerted on the dewar container due to the slosh wave excitation driven by combined gravity gradient and jitter accelerations with 10^{-6} g_o, rotating speed of 0.1 rpm, gravity turn-around time of 1200 s and gravity jitter frequency of 0.1 Hz. (A) Along x-direction fluid stress moment; (B) Along y-direction fluid stress moment; and (C) Along z-direction fluid stress moment.

Figure 16 Time sequence of the fluctuations of moment arm of fluid stress moments exerted on the dewar container driven by combined gravity gradient and jitter accelerations with 10^{-6} g_o, rotating speed of 0.1 rpm, gravity turn-around time of 1200 s and gravity jitter frequency of 0.1 Hz. (A) x-direction moment arm; (B) y-direction moment arm; and (C) z-direction moment arm.

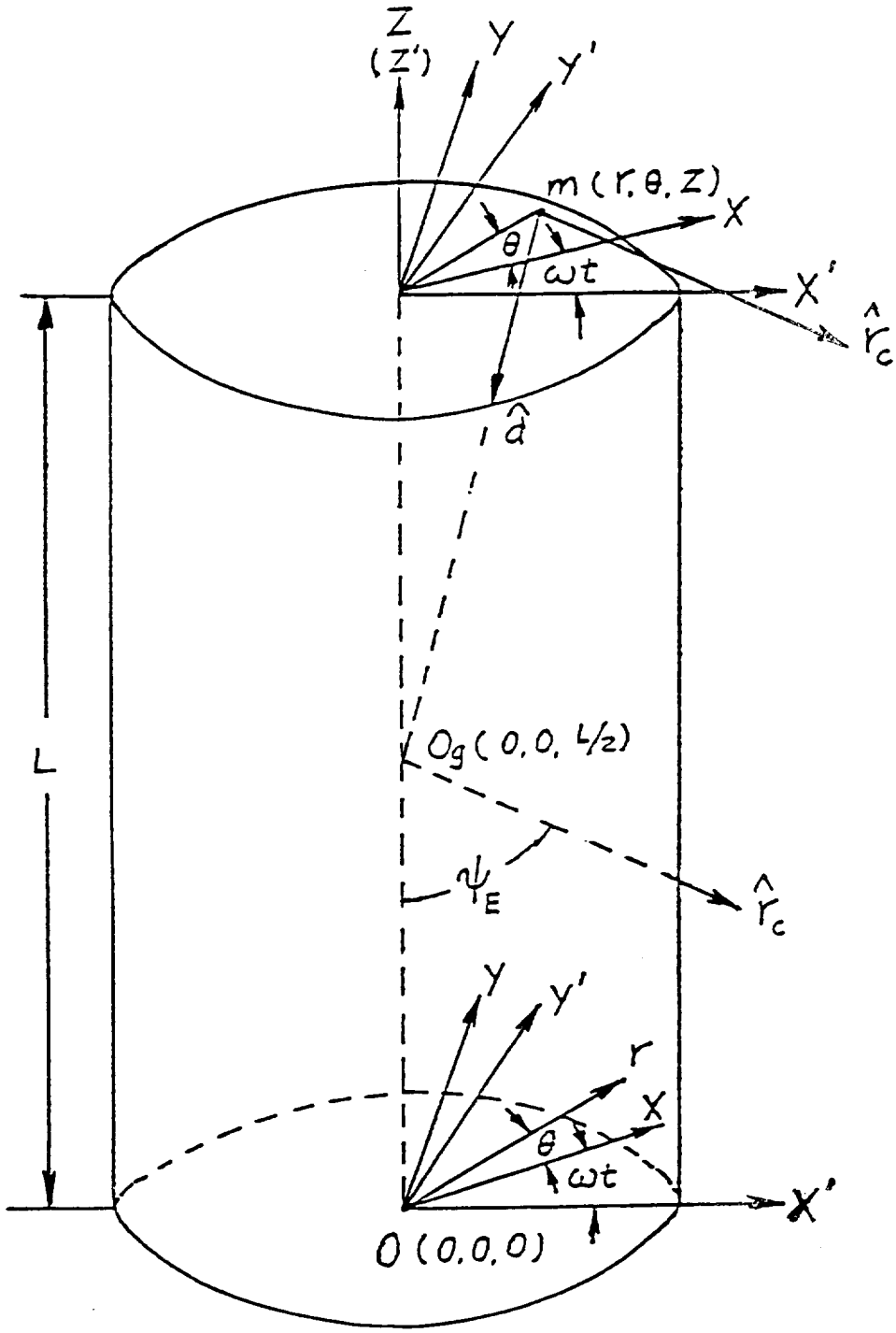
Z
(Z')
Y
Y'
m (r, θ, Z)
X
θ
ωt
X'
$\hat{r}_c$
$\hat{d}$
L
O_g (0, 0, L/2)
ψ_E
$\hat{r}_c$
Y
Y'
r
X
θ
ωt
X'
O (0, 0, 0)

Fig. 1

Time Variation of Gravity Gradient Acceleration Acting on the GP-B Spacecraft Dewar Fluid Mass Located at

(r, θ, z)

$= (40\ \text{cm}, \pi/4, 10\ \text{cm})$

$\omega = 0.1$ rpm

$\tau = 1200$ s

$g_0 = 9.81\ \text{m/s}^2$

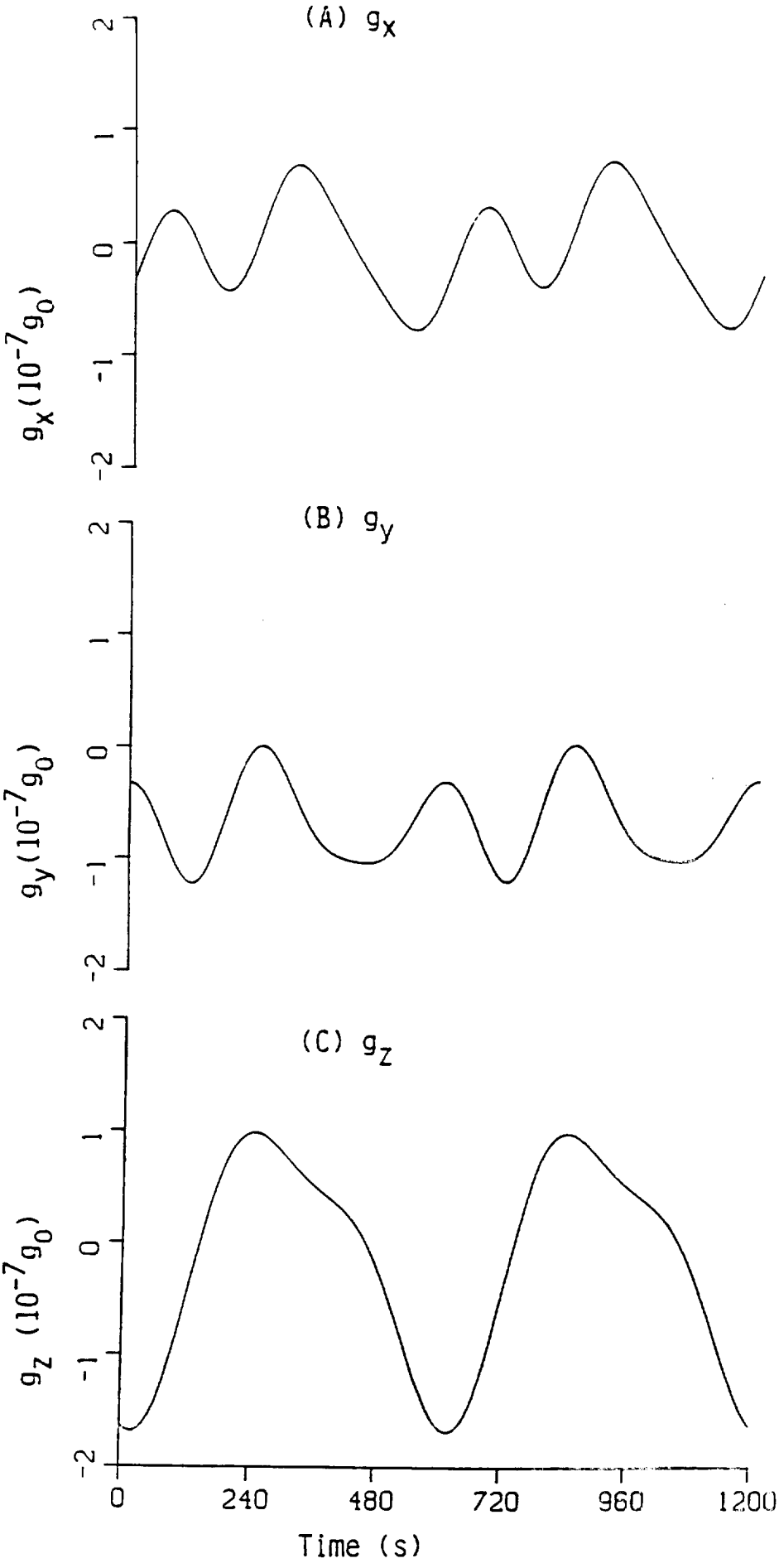

Fig. 2

Time Variation Of
Gravity Jitter
Acceleration Acting
on Spacecraft
Fluid System

$$g_B = \begin{bmatrix} 10^{-6} \\ 10^{-7} \\ 10^{-8} \end{bmatrix} g_0$$

ω = 0.1 rpm

f = 0.1 Hz

τ = 1200 s

g_0 = 9.81 m/s^2

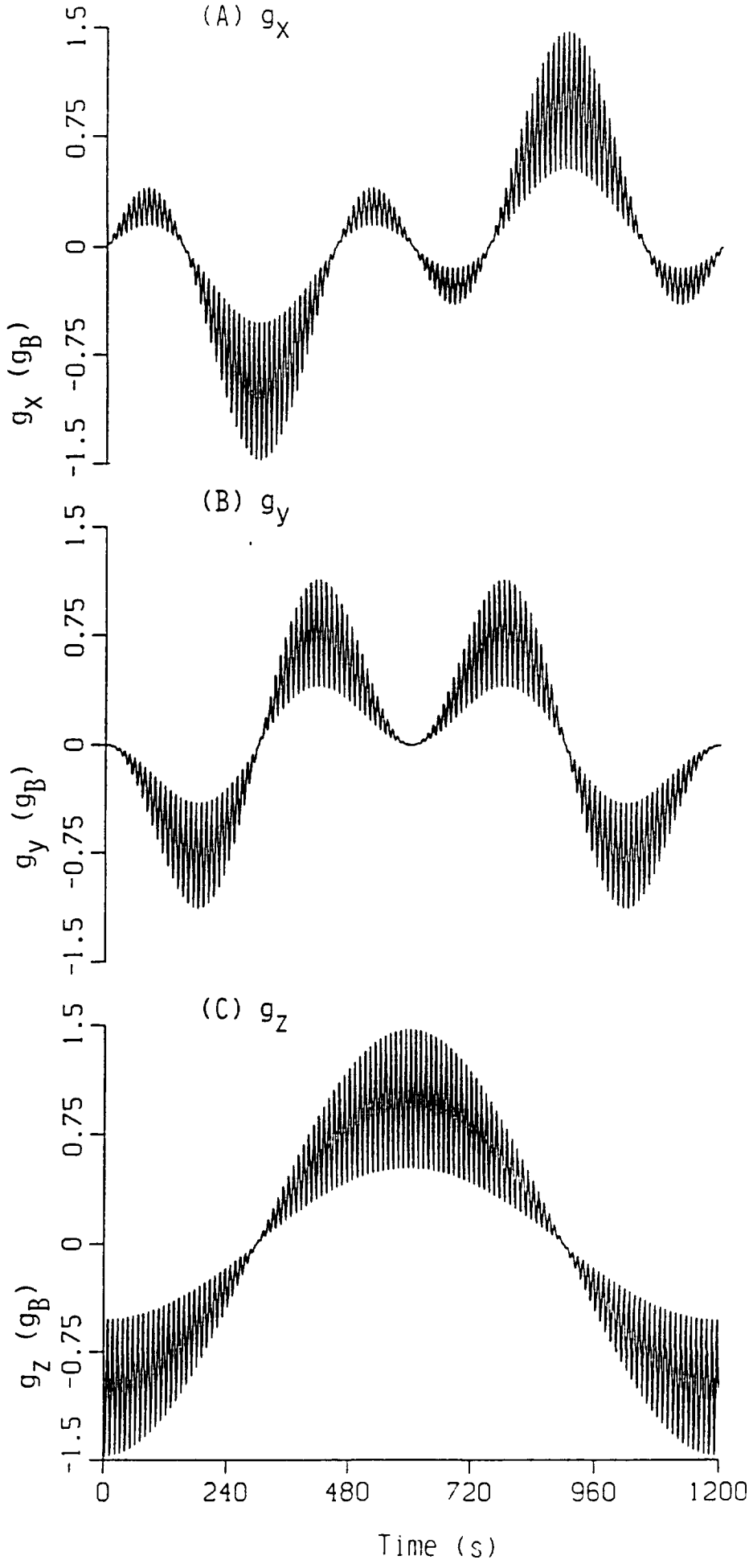

Fig. 3

INITIAL PROFILES OF LIQUID HELIUM AND VAPOR INTERFACE

Rotating Dewar Under the Effect of Gravity Jitter

$g = 10^{-7} g_0, \omega = 0.1$ rpm, $\psi_E = 0^\circ$, f = 0.1 Hz

(A) r-z plane at $\theta = 0^\circ$ and 180°

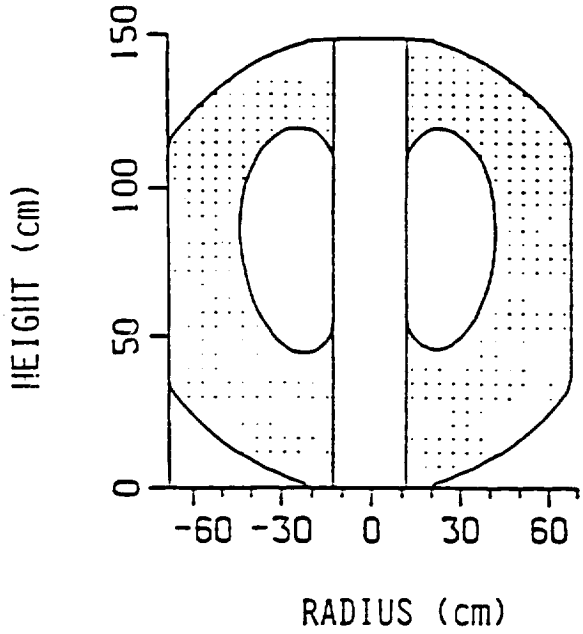

(B) r-z plane at $\theta = 90^\circ$ and 270°

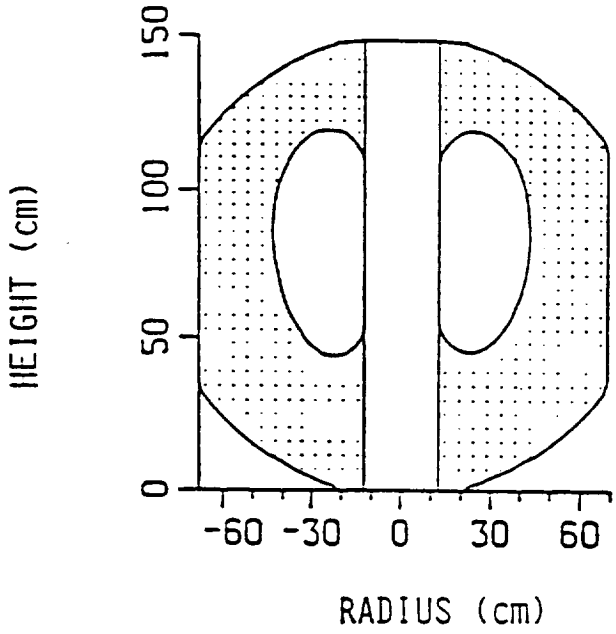

(C) r-θ plane at z = 108cm

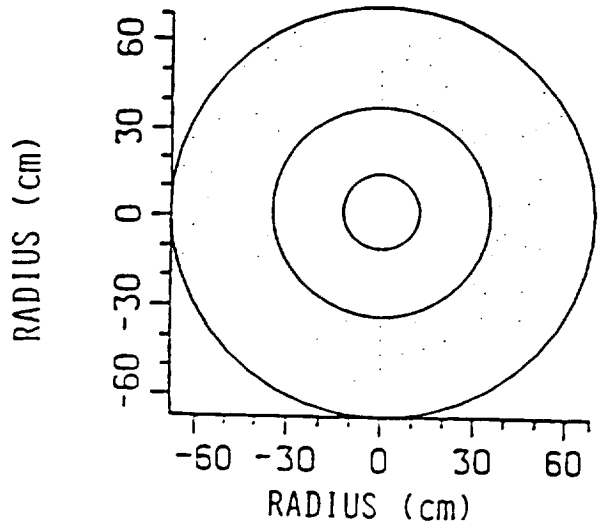

(D) Three-Dimensional Profiles

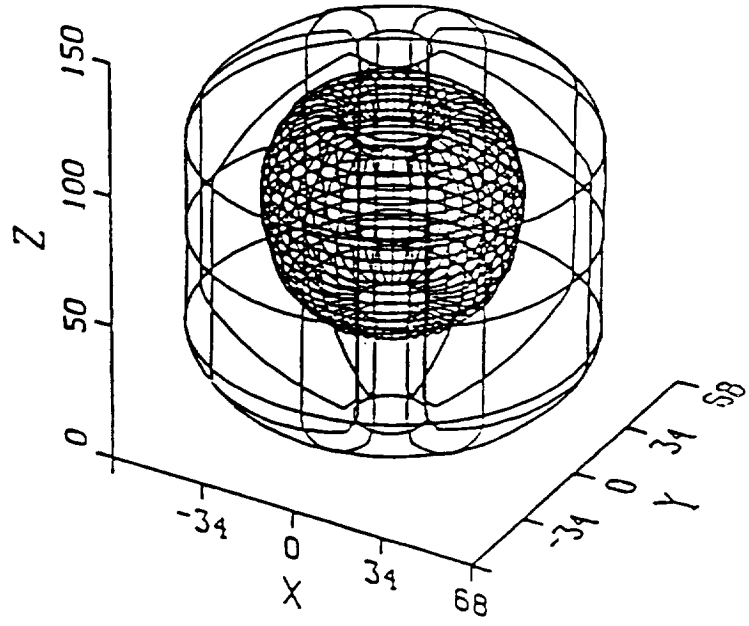

Fig. 4

THREE DIMENSIONAL LIQUID AND VAPOR INTERFACE

The Effect of Gravity Jitter and Gravity Gradient: $g = 10^{-8} g_0$

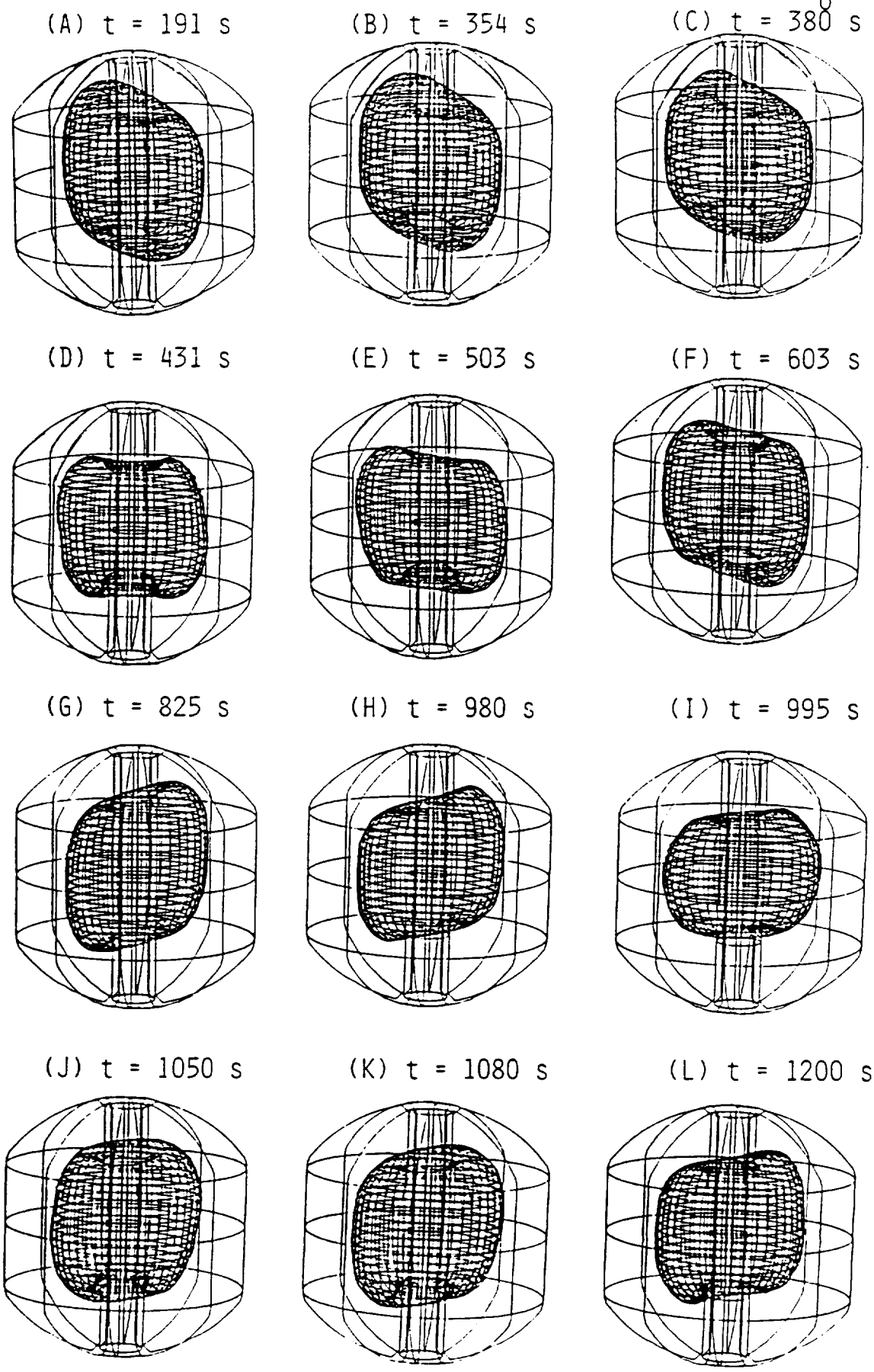

Fig. 5

THREE DIMENSIONAL LIQUID AND VAPOR INTERFACE

The Effect of Gravity Jitter and Gravity Gradient: $g = 10^{-7} g_o$

(A) t = 191 s (B) t = 354 s (C) t = 380 s

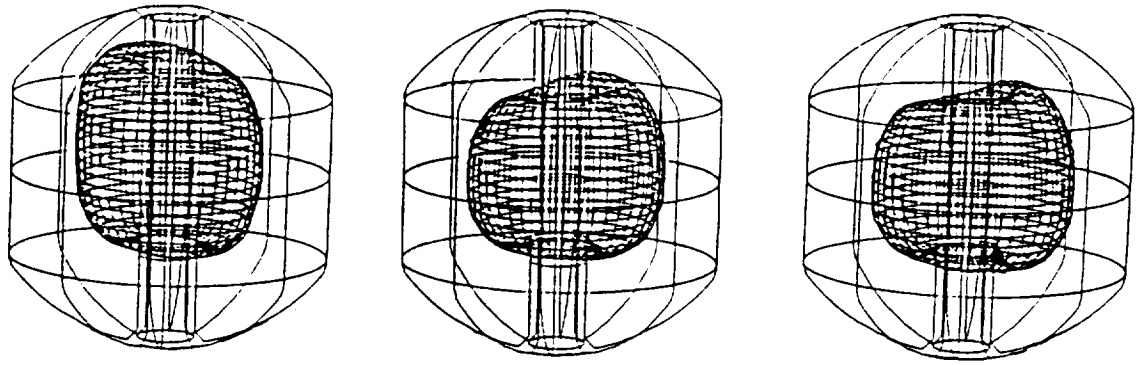

(D) t = 431 s (E) t = 503 s (F) t = 603 s

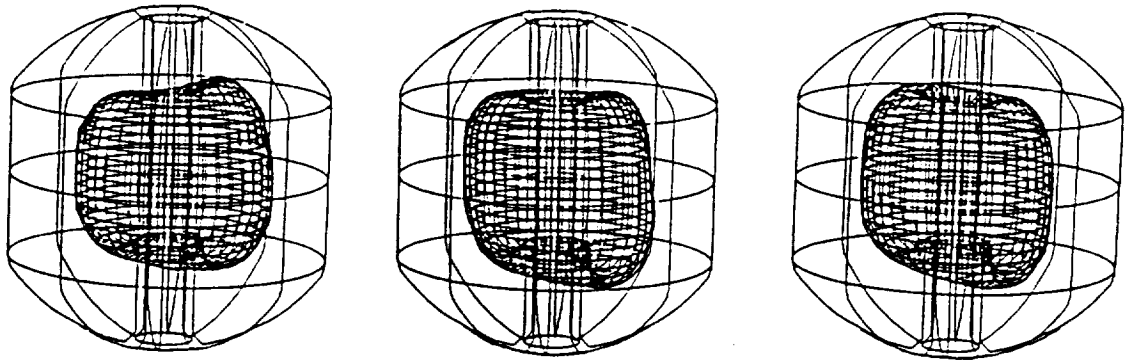

(G) t = 825 s (H) t = 980 s (I) t = 995 s

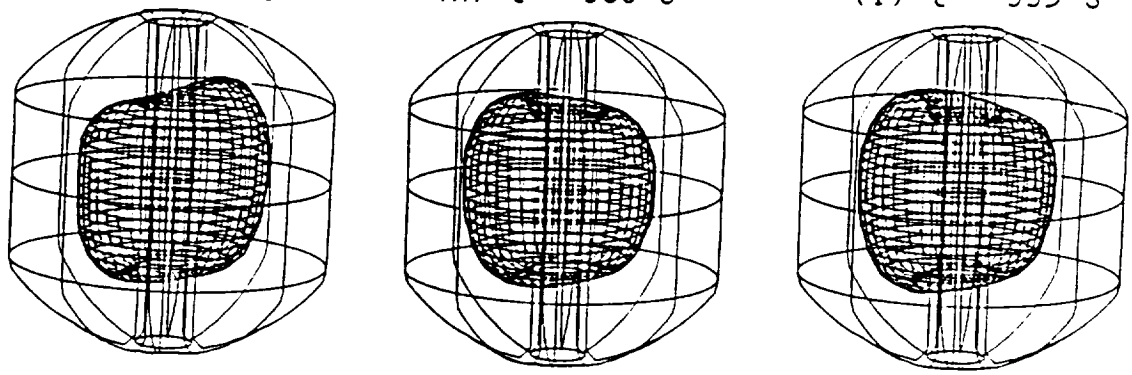

(J) t = 1050 s (K) t = 1080 s (L) t = 1200 s

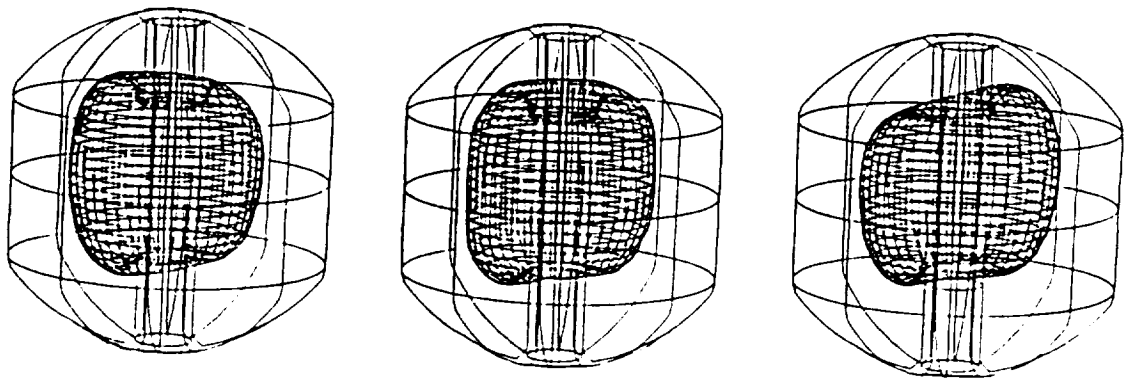

Fig. 6

THREE DIMENSIONAL LIQUID AND VAPOR INTERFACE

The Effect of Gravity Jitter and Gravity Gradient: $g = 10^{-6} g_o$

(A) t = 191 s

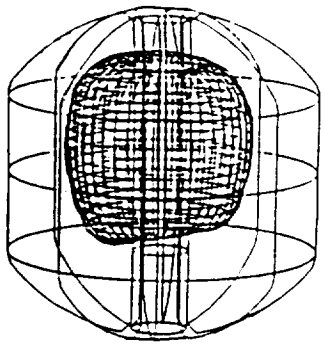

(B) t = 354 s

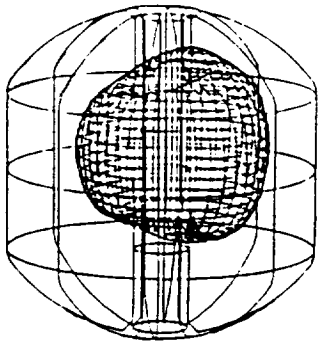

(C) t = 380 s

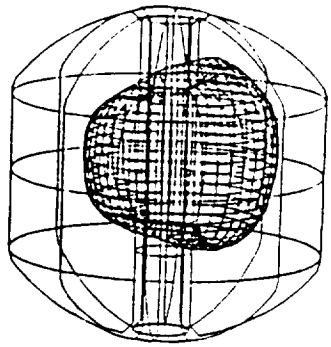

(D) t = 431 s

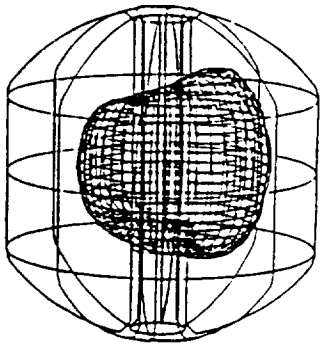

(E) t = 503 s

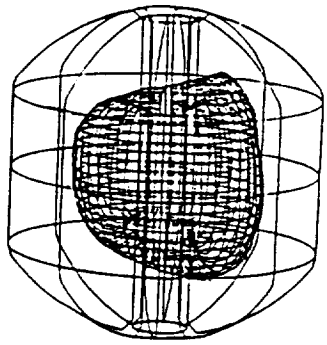

(F) t = 603 s

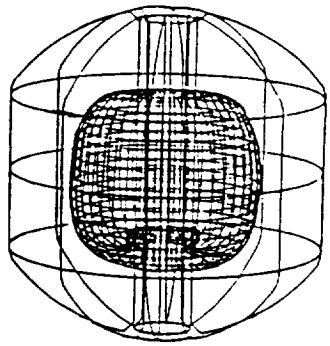

(G) t = 825 s

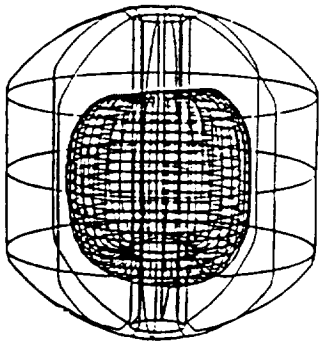

(H) t = 980 s

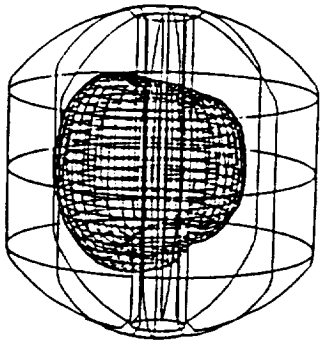

(I) t = 995 s

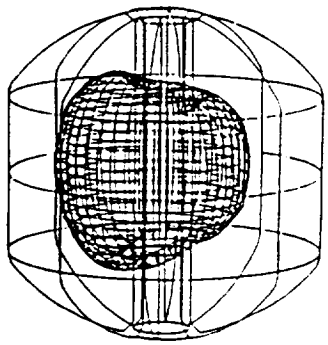

(J) t = 1050 s

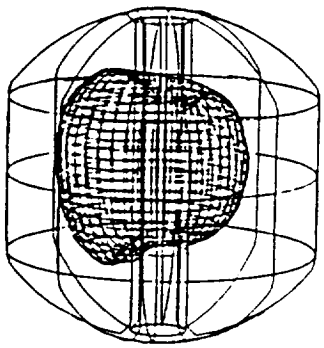

(K) t = 1080 s

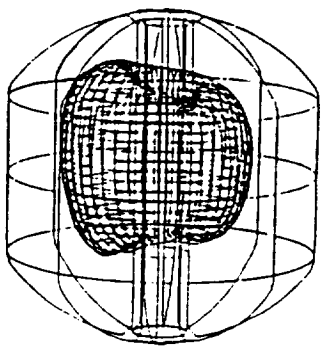

(L) t = 1200 s

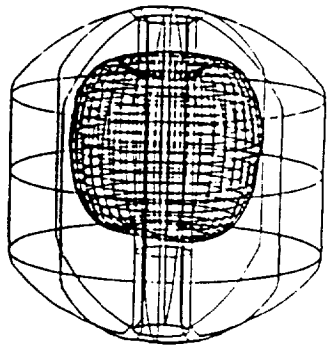

Fig. 7

VARIATIONS OF VISCOUS STRESS FORCES ACTING ON THE DEWAR TANK

(F_x, F_y, F_z)

$g = 10^{-8} g_0$

$\omega = 0.1$ rpm

$\tau = 1200$ s

f =0.1 Hz

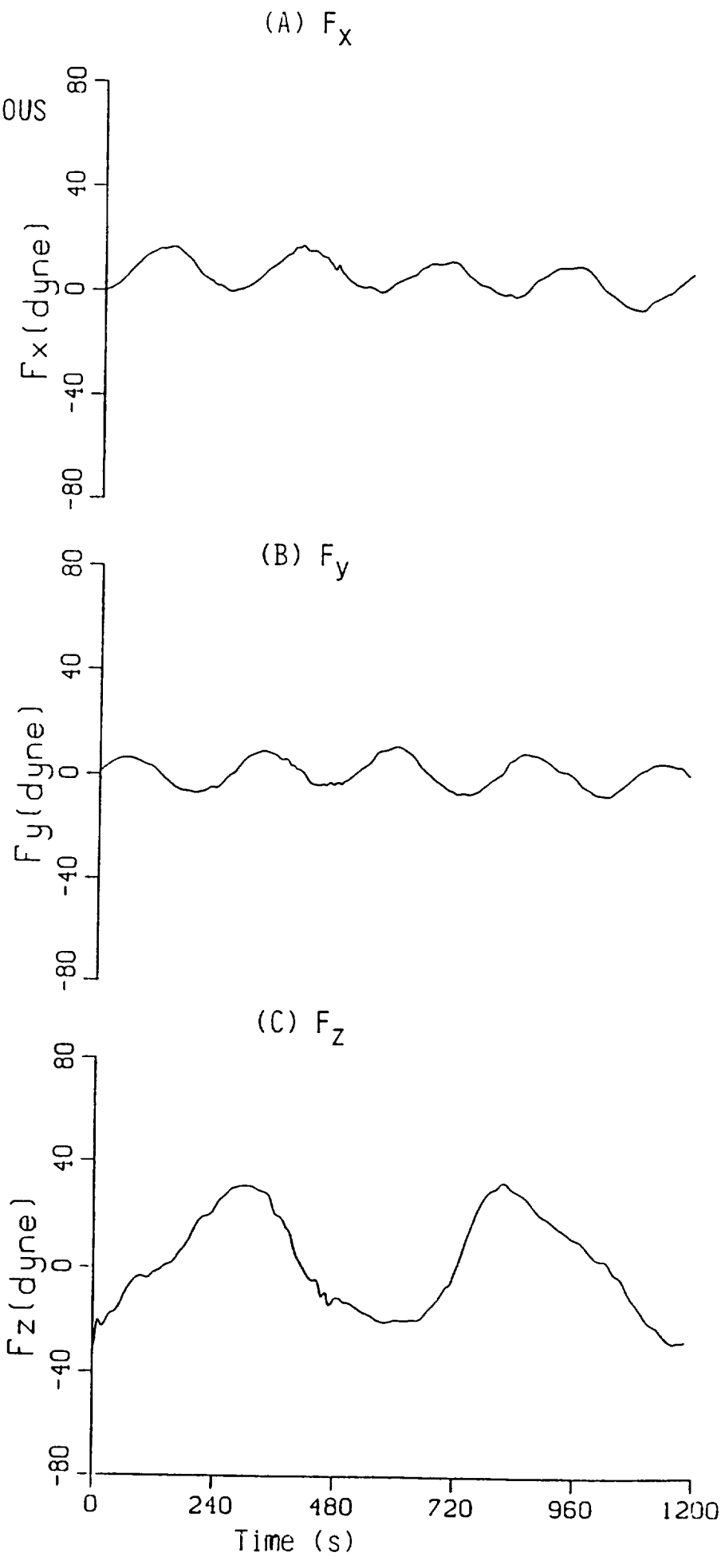

Fig. 8

VARIATIONS OF VISCOUS STRESS MOMENTS ACTING ON THE DEWAR TANK

(M_x, M_y, M_z)

$g = 10^{-8} g_0$

$\omega = 0.1$ rpm

$\tau = 1200$ s

$f = 0.1$ Hz

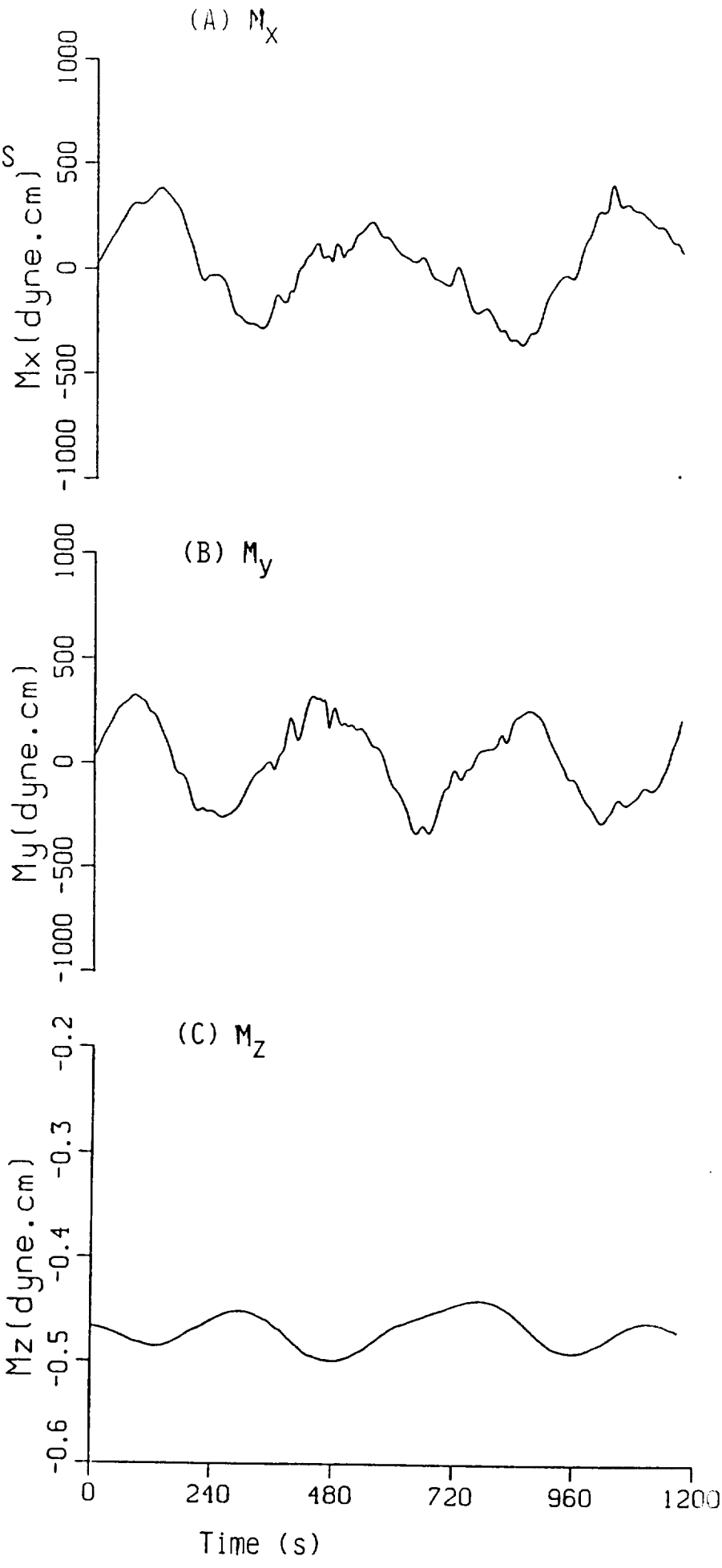

Fig 9

VARIATIONS OF MOMENT ARMS OF VISCOUS MOMENT ACTING ON THE DEWAR TANK

(L_x, L_y, L_z)

$g = 10^{-8} g_0$

$\omega = 0.1$ rpm

$\tau = 1200$ s

$f = 0.1$ Hz

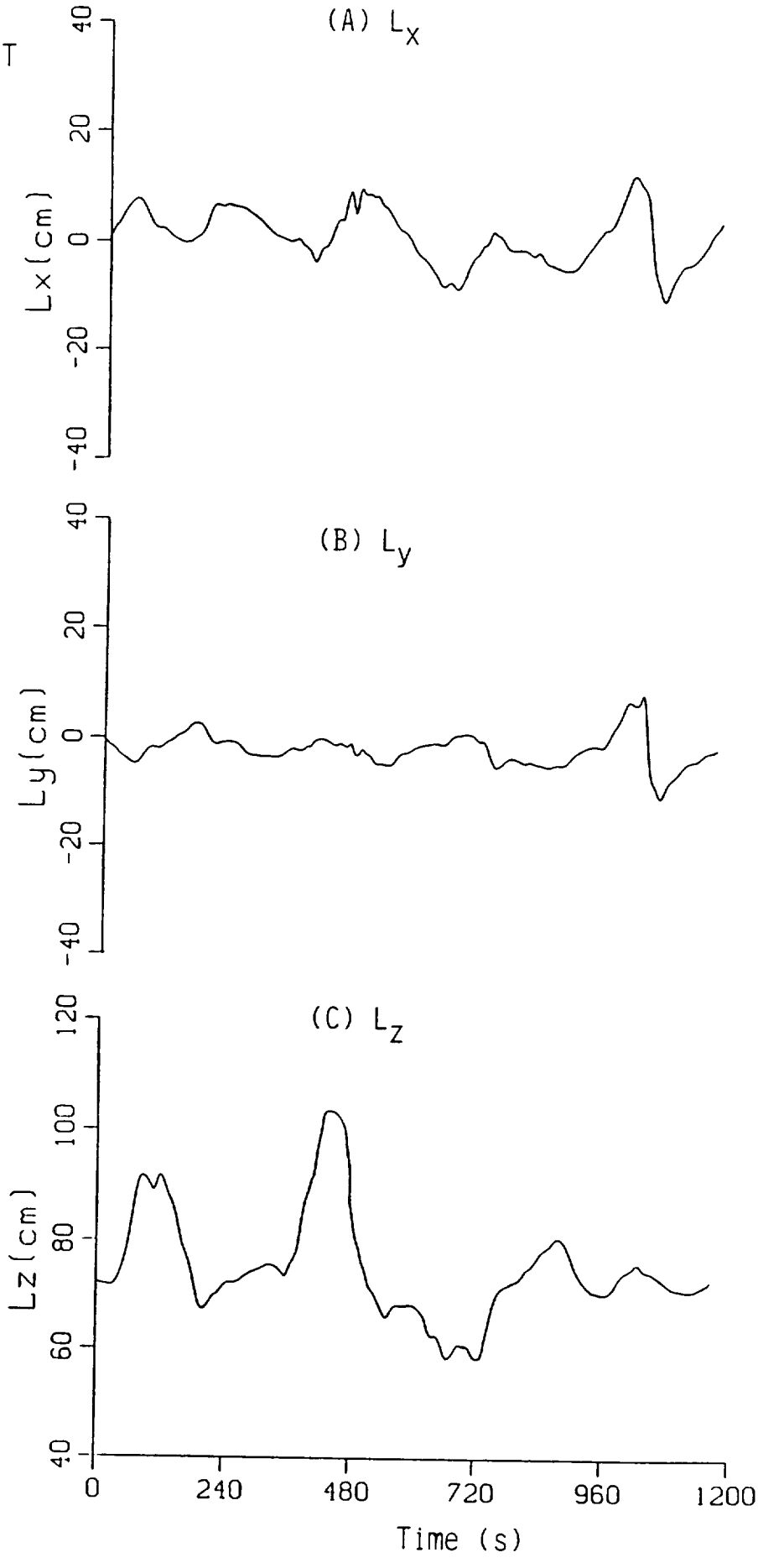

Fig. 10

VARIATIONS OF VISCOUS STRESS FORCES ACTING ON THE DEWAR TANK

(F_x, F_y, F_z)

$g = 10^{-7} g_0$

$\omega = 0.1$ rpm

$\tau = 1200$ s

$f = 0.1$ Hz

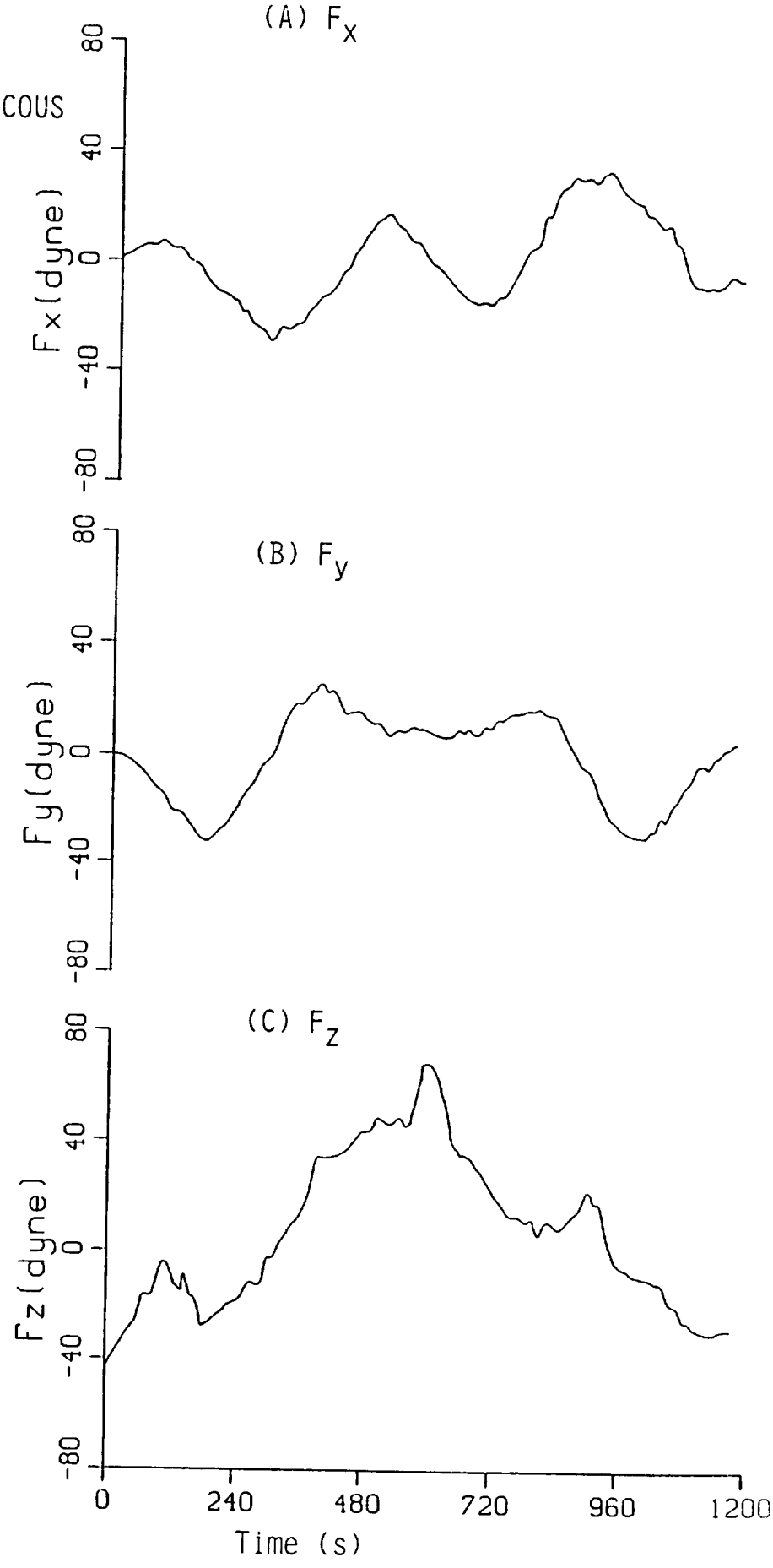

Fig. 11

VARIATIONS OF VISCOUS STRESS MOMENTS ACTING ON THE DEWAR TANK

(M_x, M_y, M_z)

$g = 10^{-7} g_0$

$\omega = 0.1$ rpm

$\tau = 1200$ s

$f = 0.1$ Hz

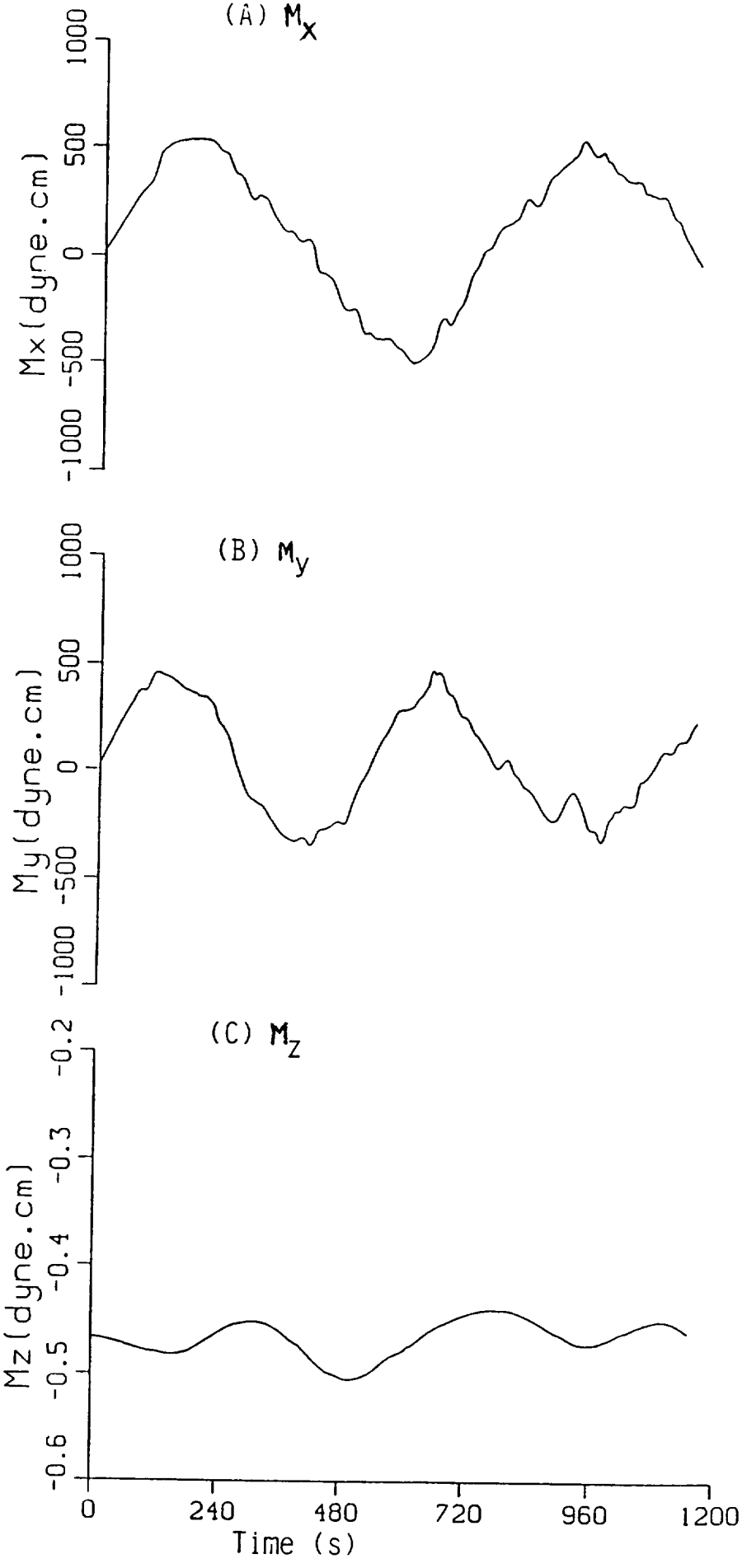

Fig. 12

VARIATIONS OF MOMENT ARMS OF VISCOUS STRESS MOMENT ACTING ON THE DEWAR TANK

(L_x, L_y, L_z)

$g = 10^{-7} g_0$

$\omega = 0.1$ rpm

$\tau = 1200$ s

$f = 0.1$ Hz

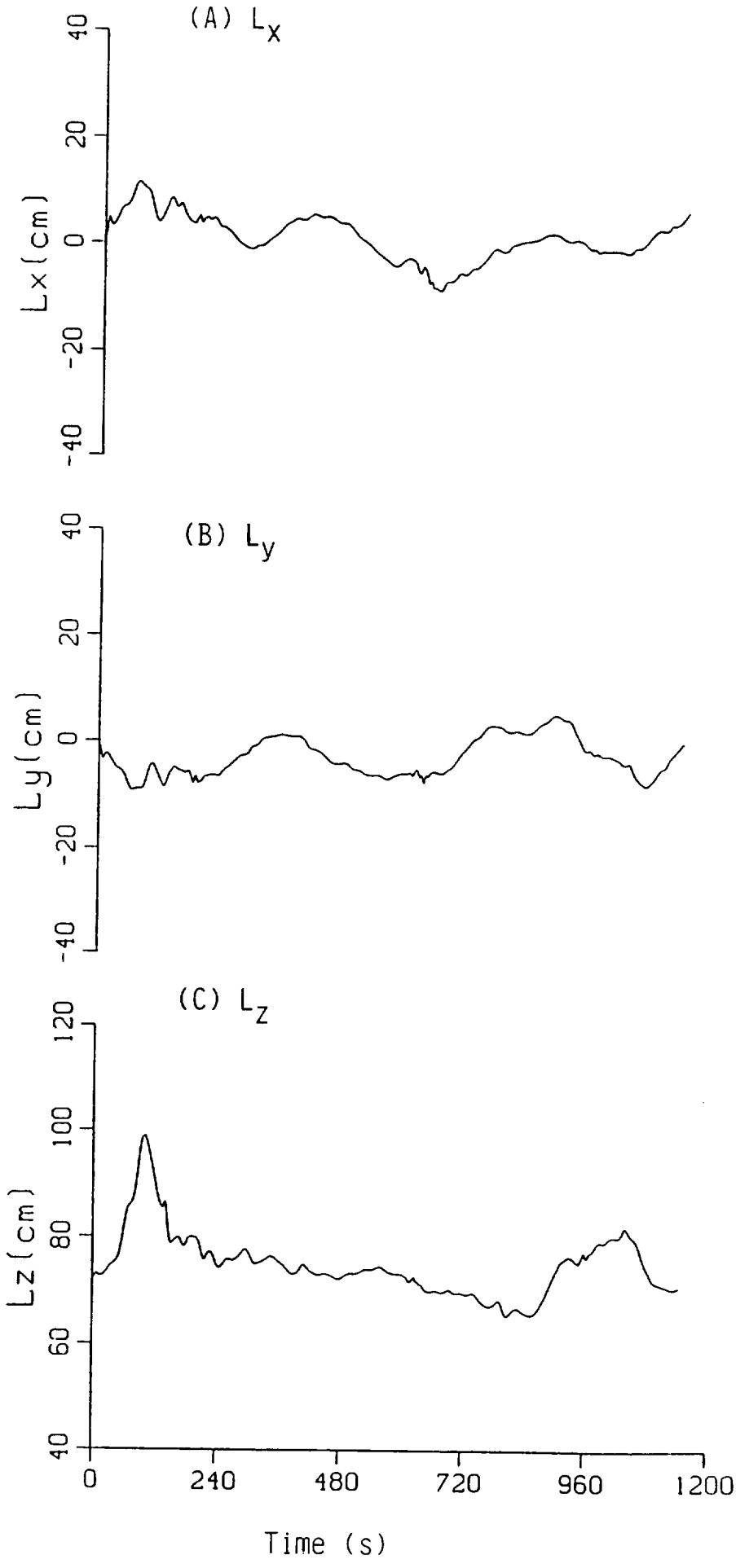

Fig. 13

VARIATIONS OF VISCOUS
STRESS FORCES
ACTING ON
THE DEWAR TANK

(F_x, F_y, F_z)

$g = 10^{-6} g_0$

$\omega = 0.1$ rpm

$\tau = 1200$ s

$f = 0.1$ Hz

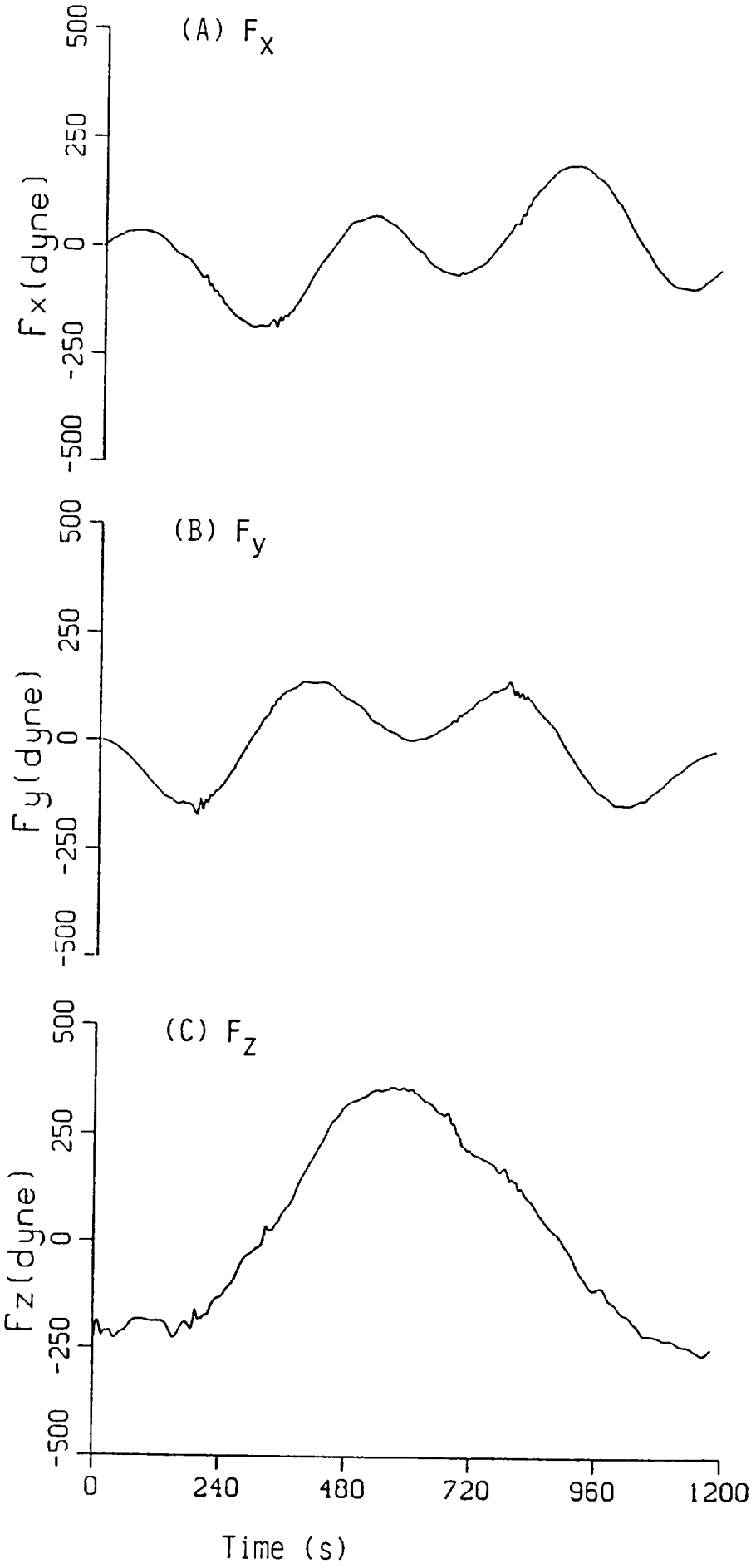

Fig. 14

VARIATIONS OF VISCOUS STRESS MOMENTS ACTING ON THE DEWAR TANK

(M_x, M_y, M_z)

$g = 10^{-6} g_0$

$\omega = 0.1$ rpm

$\tau = 1200$ s

$f = 0.1$ Hz

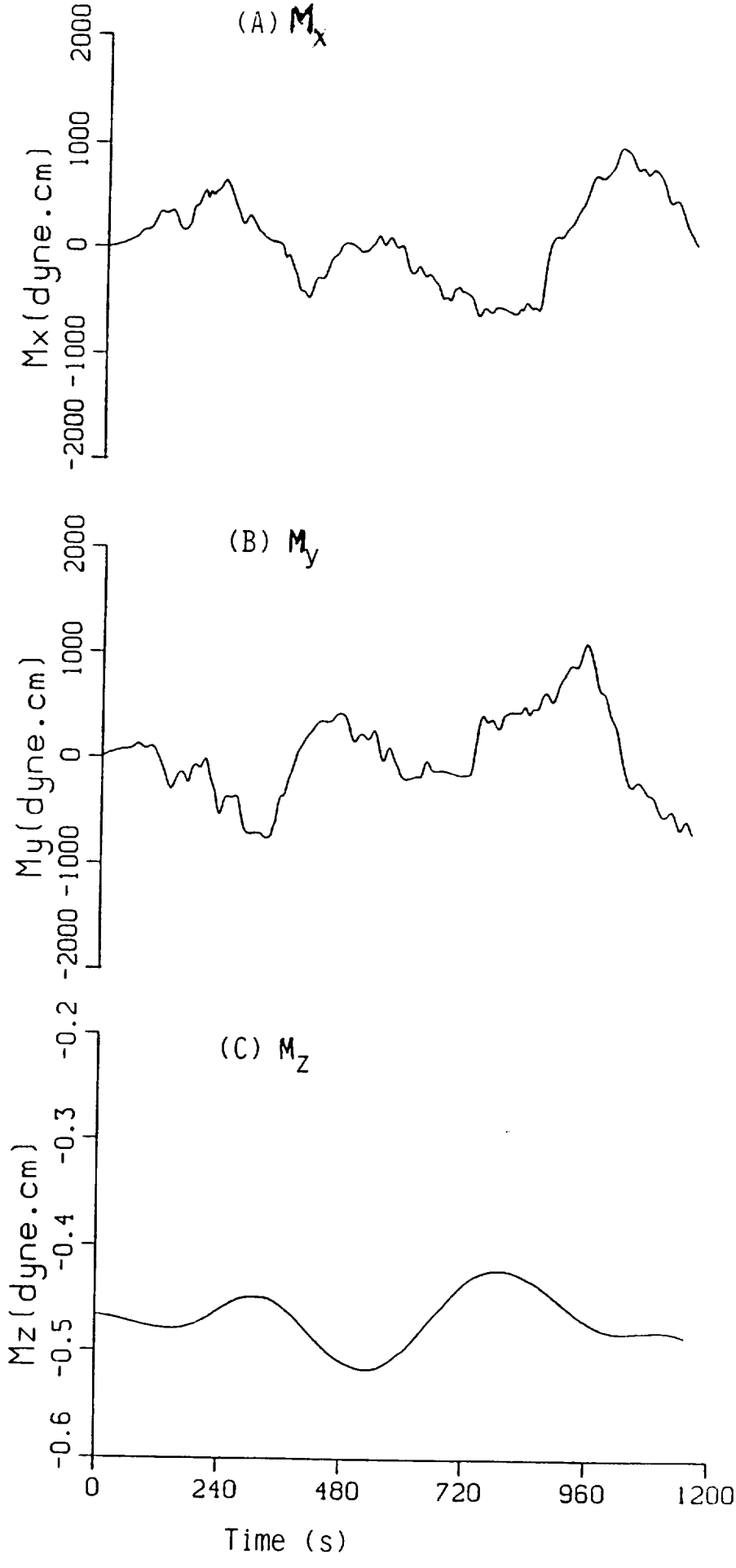

Fig. 15

VARIATIONS OF MOMENT ARMS OF VISCOUS STRESS MOMENT ACTING ON THE DEWAR TANK

(L_x, L_y, L_z)

$g = 10^{-6} g_o$

$\omega = 0.1$ rpm

$\tau = 1200$ s

$f = 0.1$ Hz

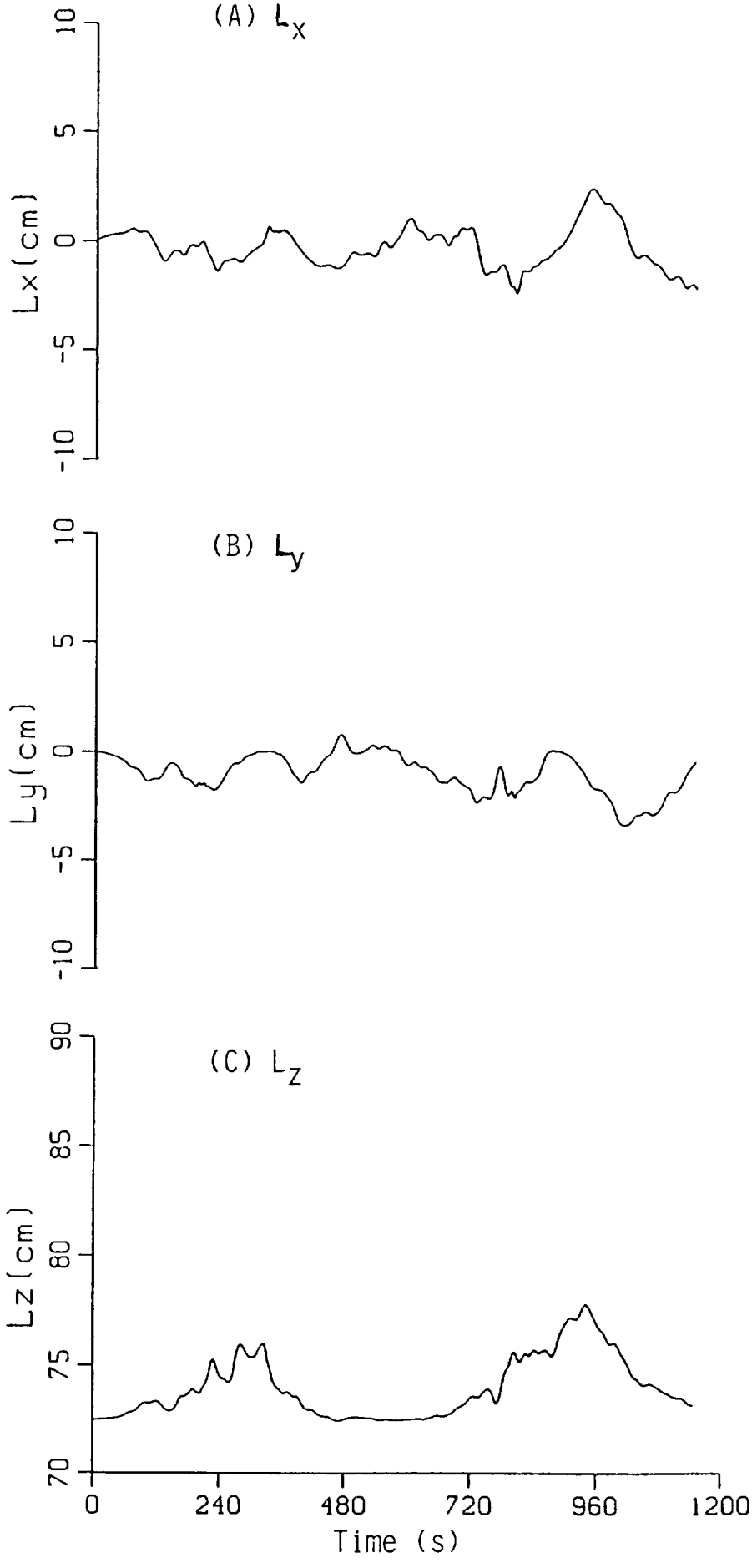

Fig. 16